2025/5/1-2 postQM2025

流体・動的模型(理論)

Hydro and Dynamical model

SOPHIA HADRON PHYSICS GROUP

Shin-ei Fujii

Sophia University

Topics

- Causality and stability in hydrodynamics (L. Gavassino)
- 3D Bayesian analysis (A. Mankolli, T. S. Domingues)
- Nuclear structure in high-energy collisions (G. H. Nijs, C. Shen)
- Rapidity scan with DCCI at LHC energy (S. Fujii)

Topics

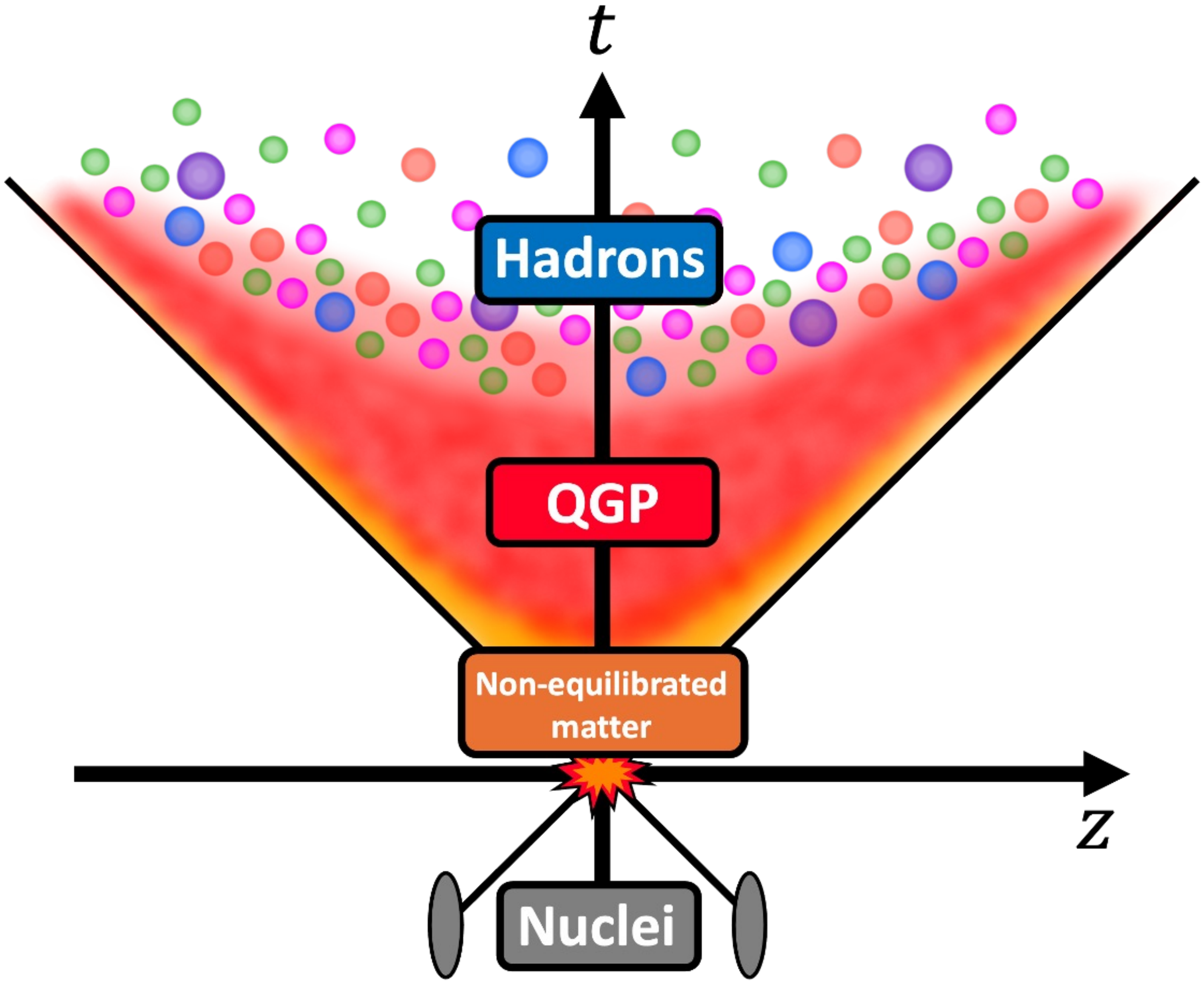

Topics

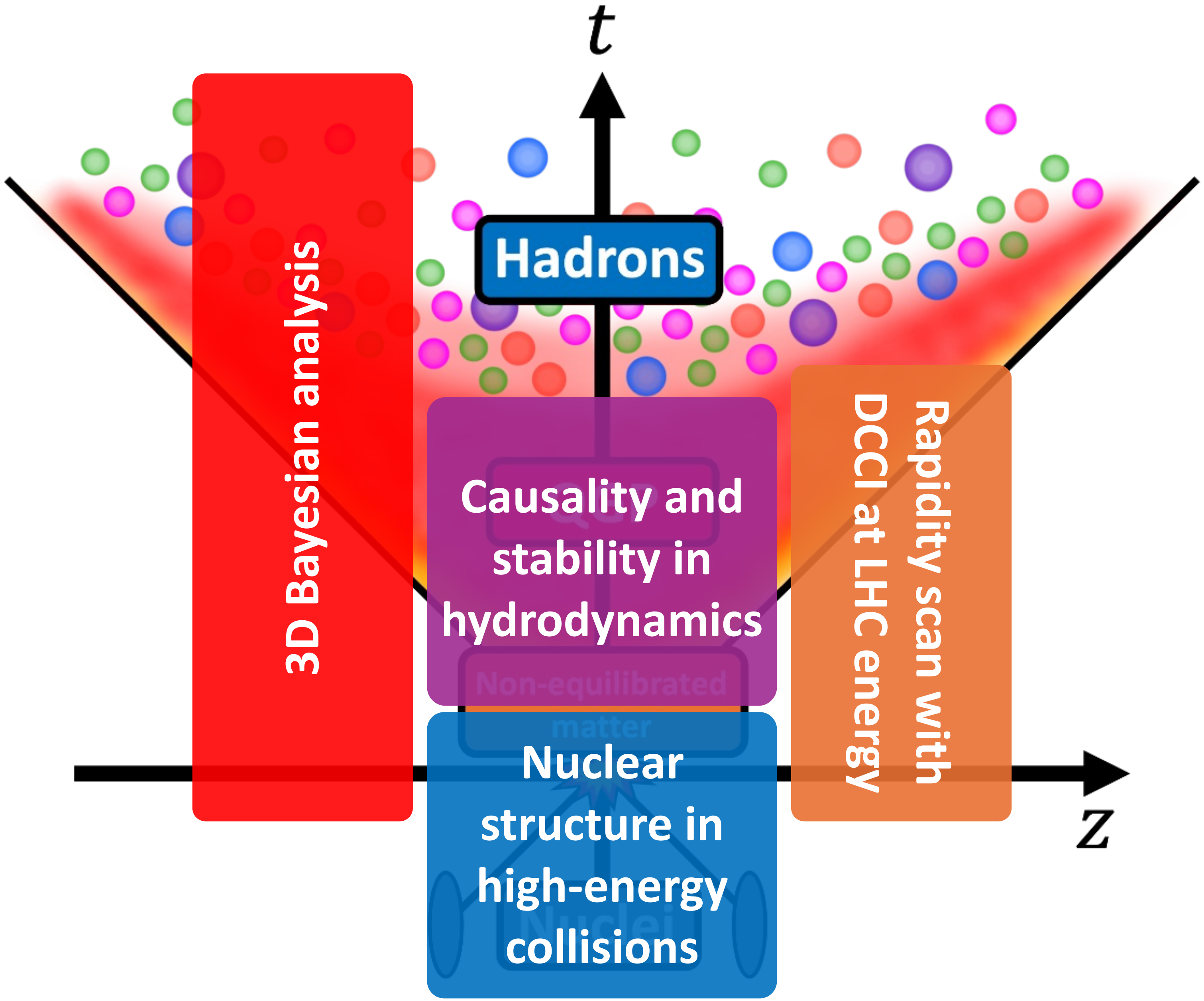
t
3D Bayesian analysis
Hadrons
Causality and stability in hydrodynamics
Non-equilibrated matter
Nuclear structure in high-energy collisions
Rapidity scan with DCCI at LHC energy
z

Causality and stability in hydrodynamics

Based on:

Lorenzo Gavassino (parallel 12, Tue)

What is causality?

L. Gavassino

SOPHIA HADRON PHYSICS GROUP

Alice cannot use the fluid to send information to Bob faster than light

1. Alice perturbs the fluid at her location
2. The induced changes travel inside an “acoustic cone”
3. This cone should be contained inside the light cone

$$w \leq c \, (= 1)$$

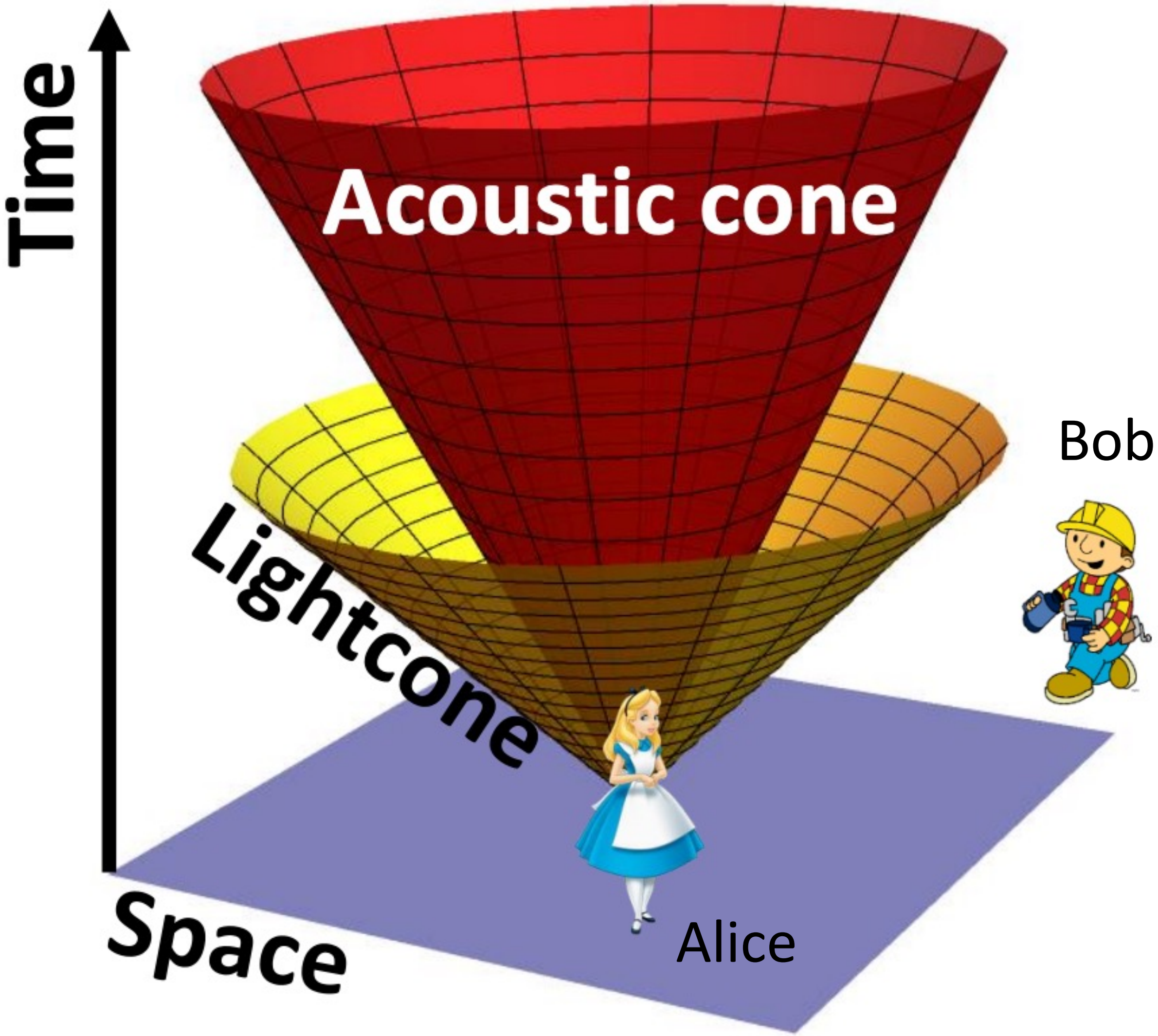

w: characteristic velocity (local velocity of information)
c: speed of light

w in relativistic hydrodynamics

L. Gavassino

SOPHIA HADRON PHYSICS GROUP

w = speed of sound + diffusion

- **Ideal fluid**

$$w^2 = c_s^2$$

c_s: sound velocity

- **Ideal fluid + Bulk pressure (near equilibrium)**

$$w^2 = c_s^2 + \frac{\zeta}{\tau_\Pi(e+P)}$$

Hiscock-Lindblom (1983)

ζ: bulk viscosity

τ_Π: relaxation time

- **Ideal fluid + Bulk pressure (far from equilibrium)**

$$w^2 = c_s^2 + \frac{\zeta}{\tau_\Pi(e+P+\Pi)}$$

Bemfica-Disconzi-Noronha (2019)

Π: bulk pressure

Problem

In Navier-Stokes limit,

$$\Pi = -\zeta\theta, \quad \theta \approx \frac{1}{\tau}$$

θ: expansion scalar

τ: proper time

$\Downarrow$

Π can approach to $-(e+P)$ in early time

$\Downarrow$

$w \to \infty$ (acausality)!

Causality violation in hydrodynamic model

L. Gavassino

SOPHIA HADRON PHYSICS GROUP

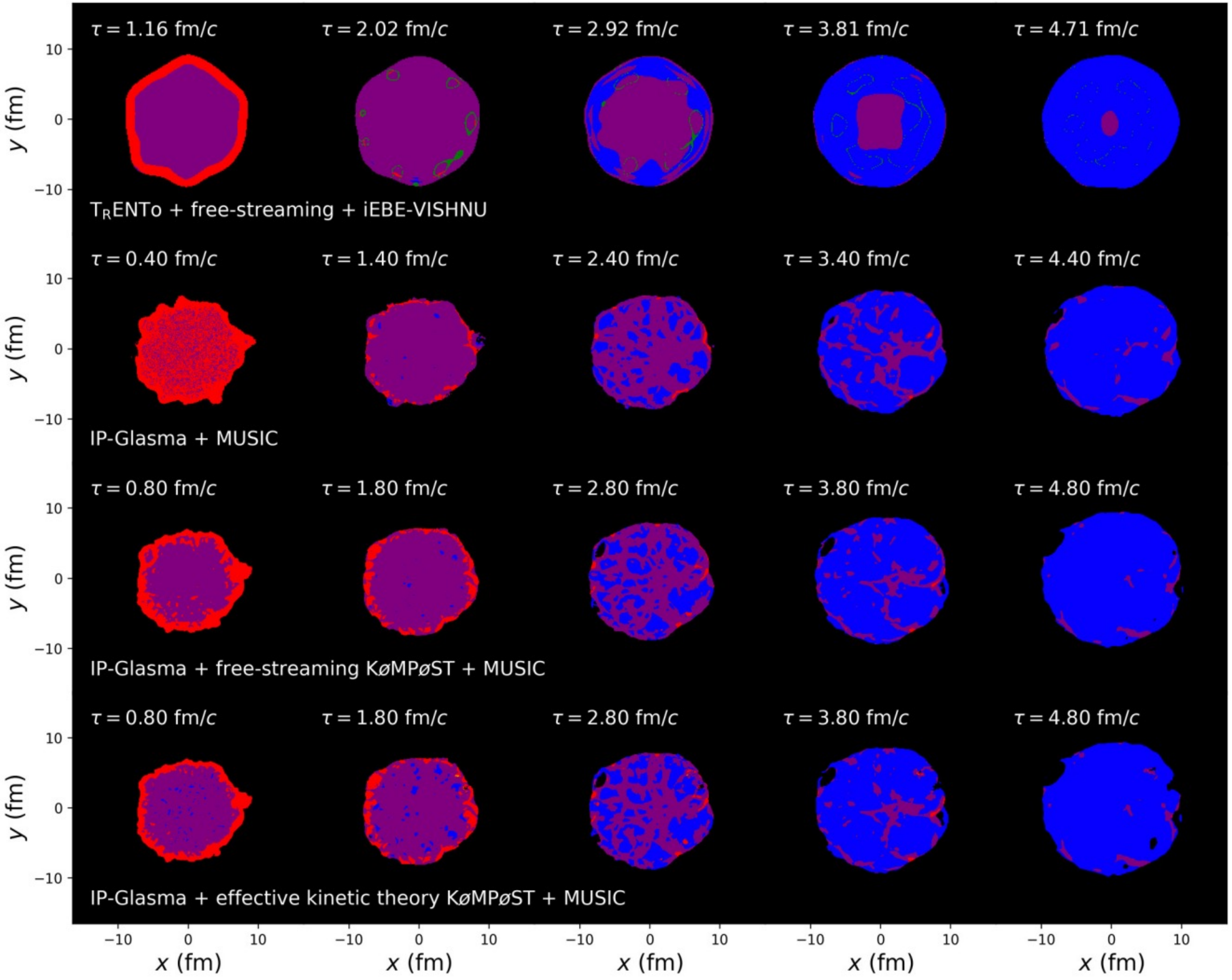

Red: acausal

Purple: unknown

Blue: causal

Plumberg *et al.* (2022)

Causality violations are not rare...

What happens?

What happens?

L. Gavassino

v: fluid velocity

① Acausal ($w > 1$) but small v

Specifically, $wv < 1$

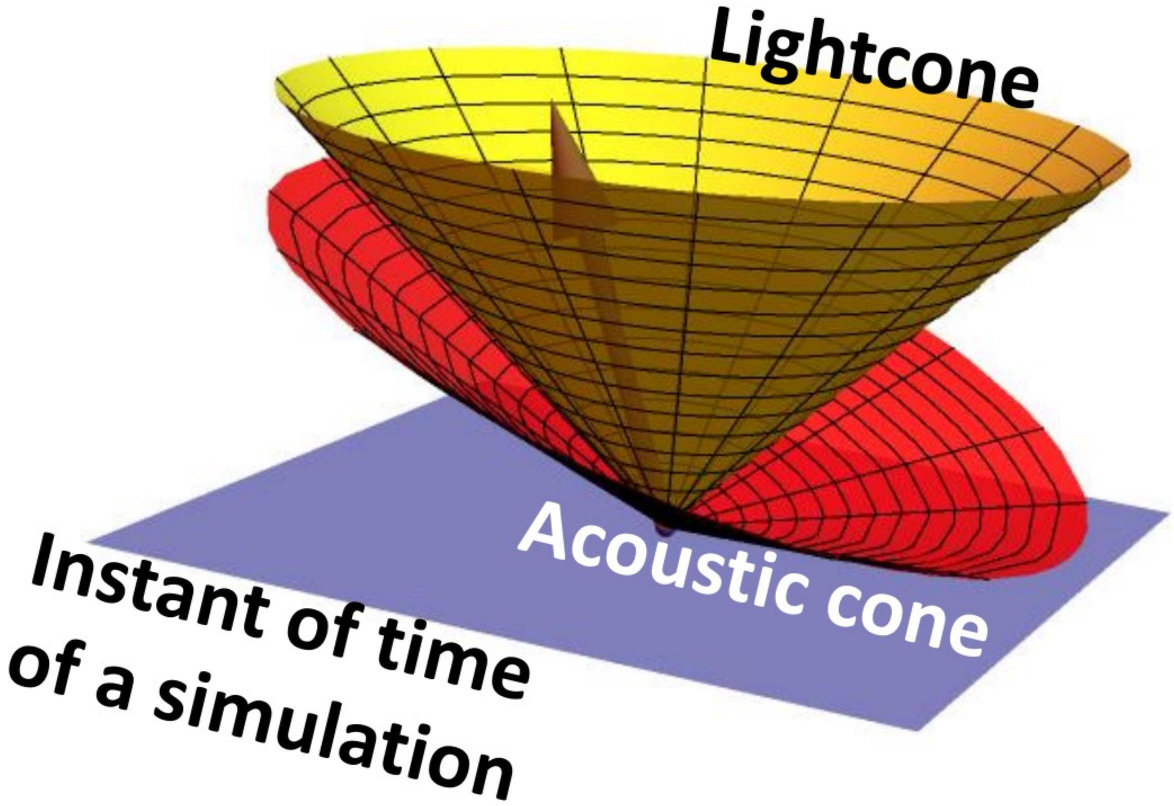

② Acausal ($w > 1$) and large v

Specifically, $wv \geq 1$

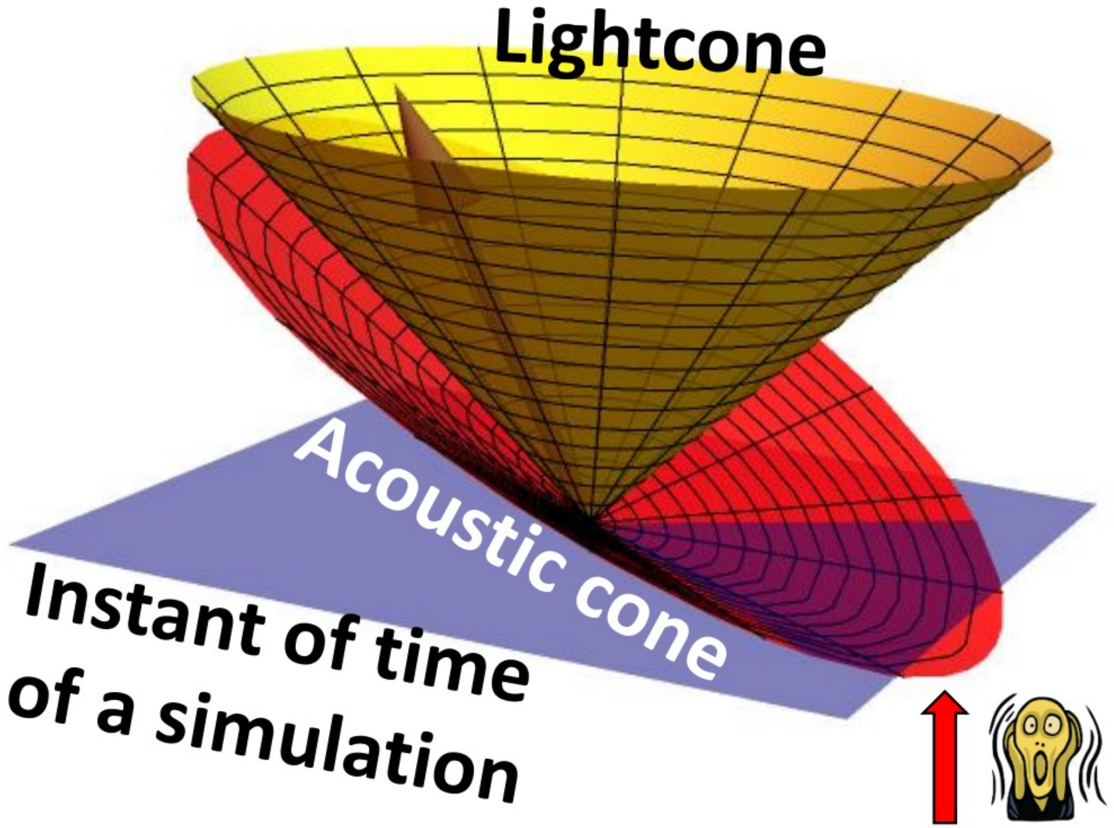

What happens?

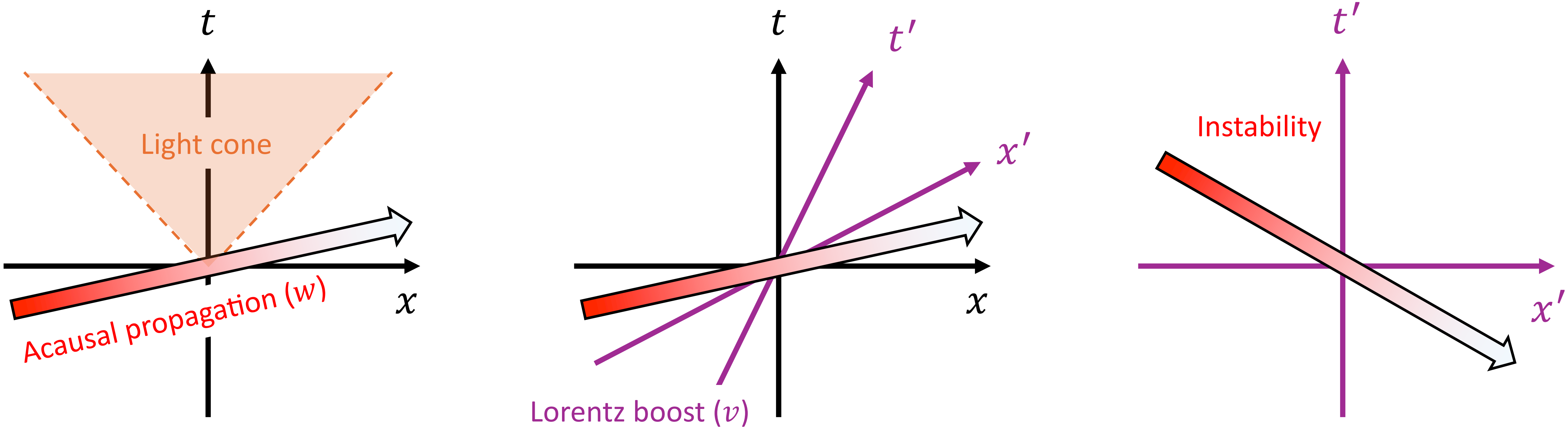

Excessive acausality ($wv \geq 1$) induces instability!!

A simple example

L. Gavassino

SOPHIA HADRON PHYSICS GROUP

Assume Israel-Stewart eq. with bulk pressure

$$(\tau_\Pi D + 1)\Pi = -\zeta\theta \qquad D = u^\mu \partial_\mu \qquad \theta = \partial_\mu u^\mu$$

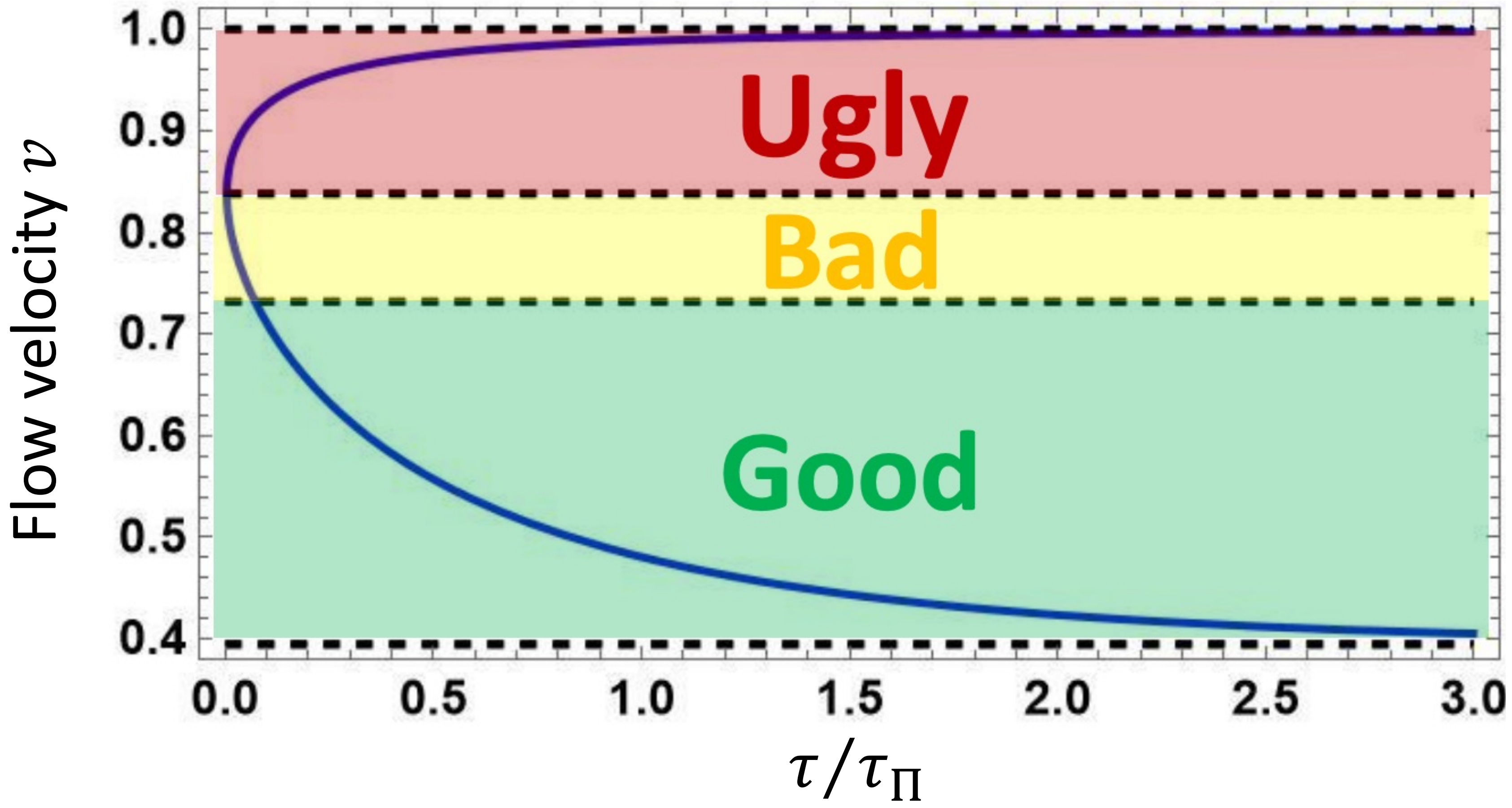

$v = 1$ (speed of light)

$wv = 1$ (stability ends)

$w = 1$ (causality ends)

$v =$ (velocity at equilibrium)

The simulation does not see the instability

L. Gavassino

SOPHIA HADRON PHYSICS GROUP

Start **Good** or **Bad**

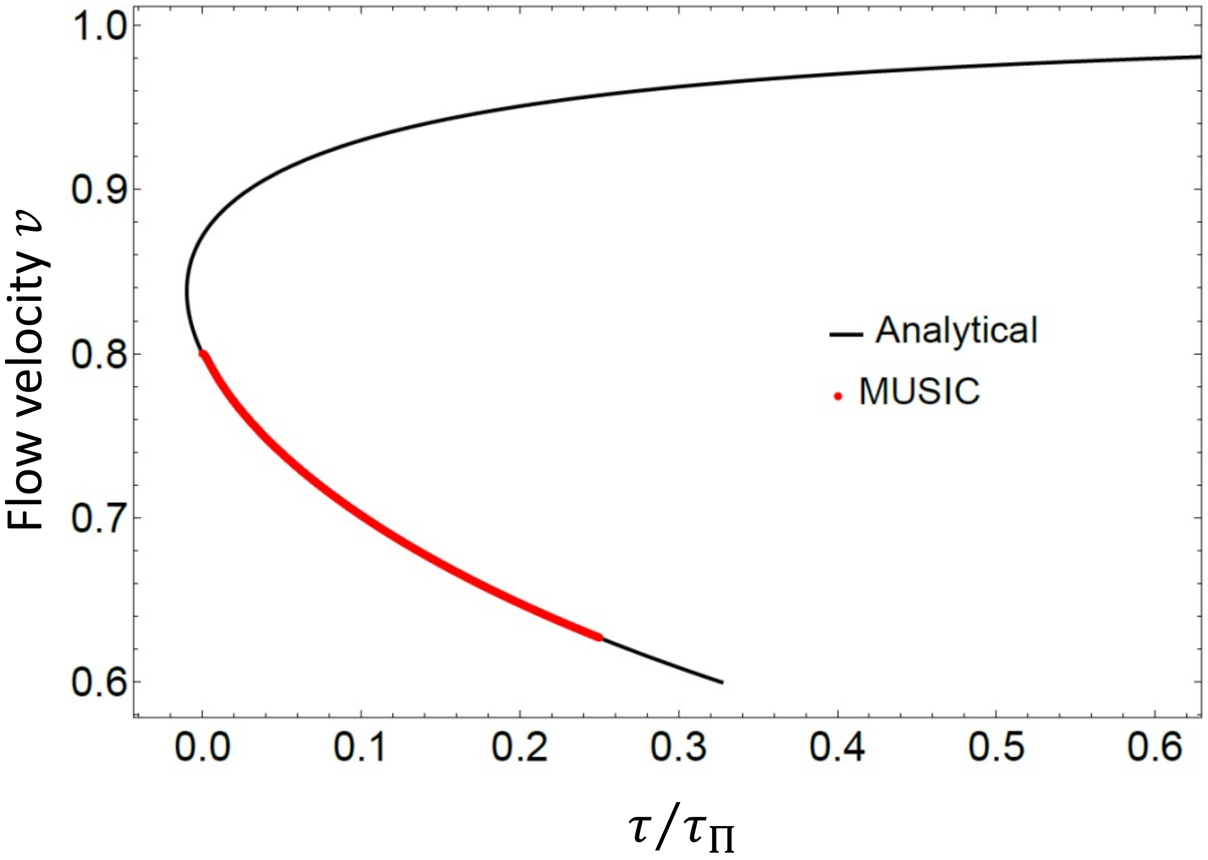

Start **Ugly**

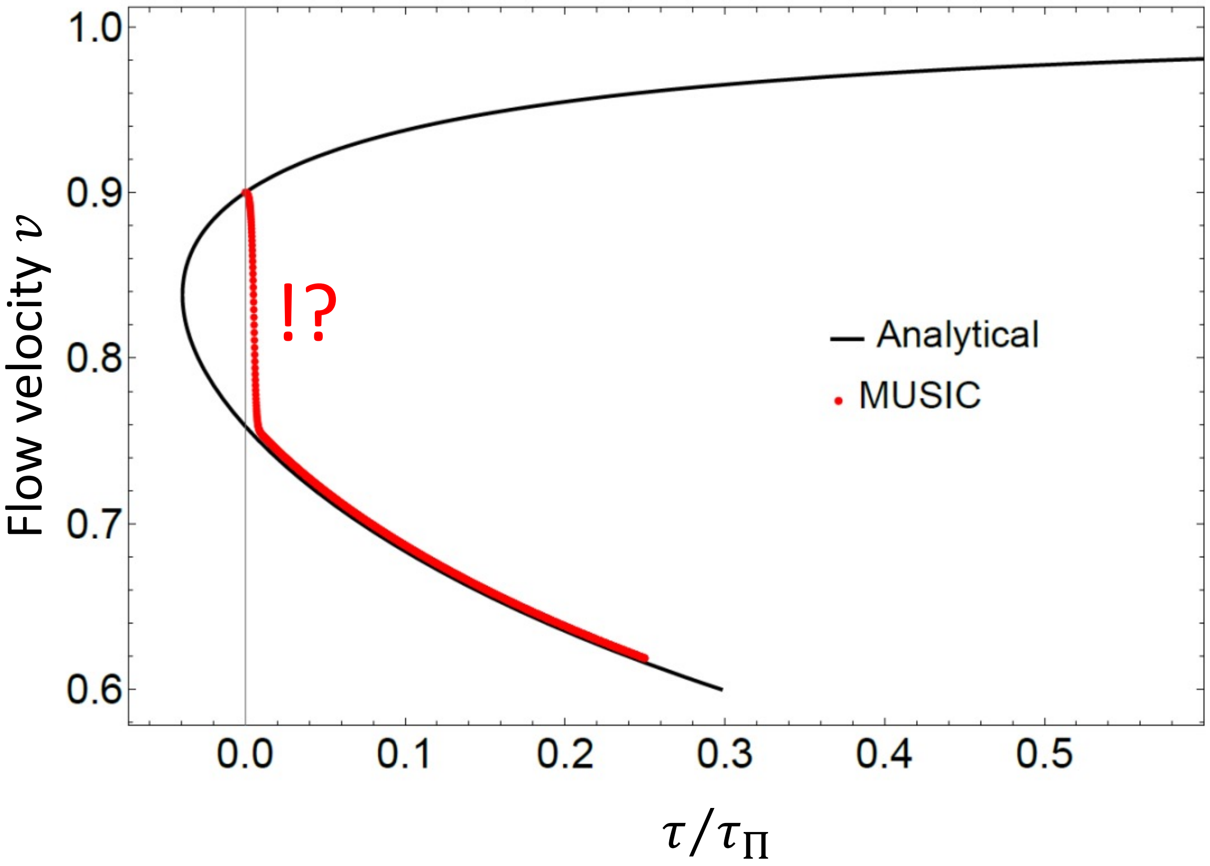

Numerical “stabilization” due to an inconsistent treatment of the derivatives in the dissipative equations

Example with MUSIC

L. Gavassino

SOPHIA HADRON PHYSICS GROUP

Numerical solution with correct initialization

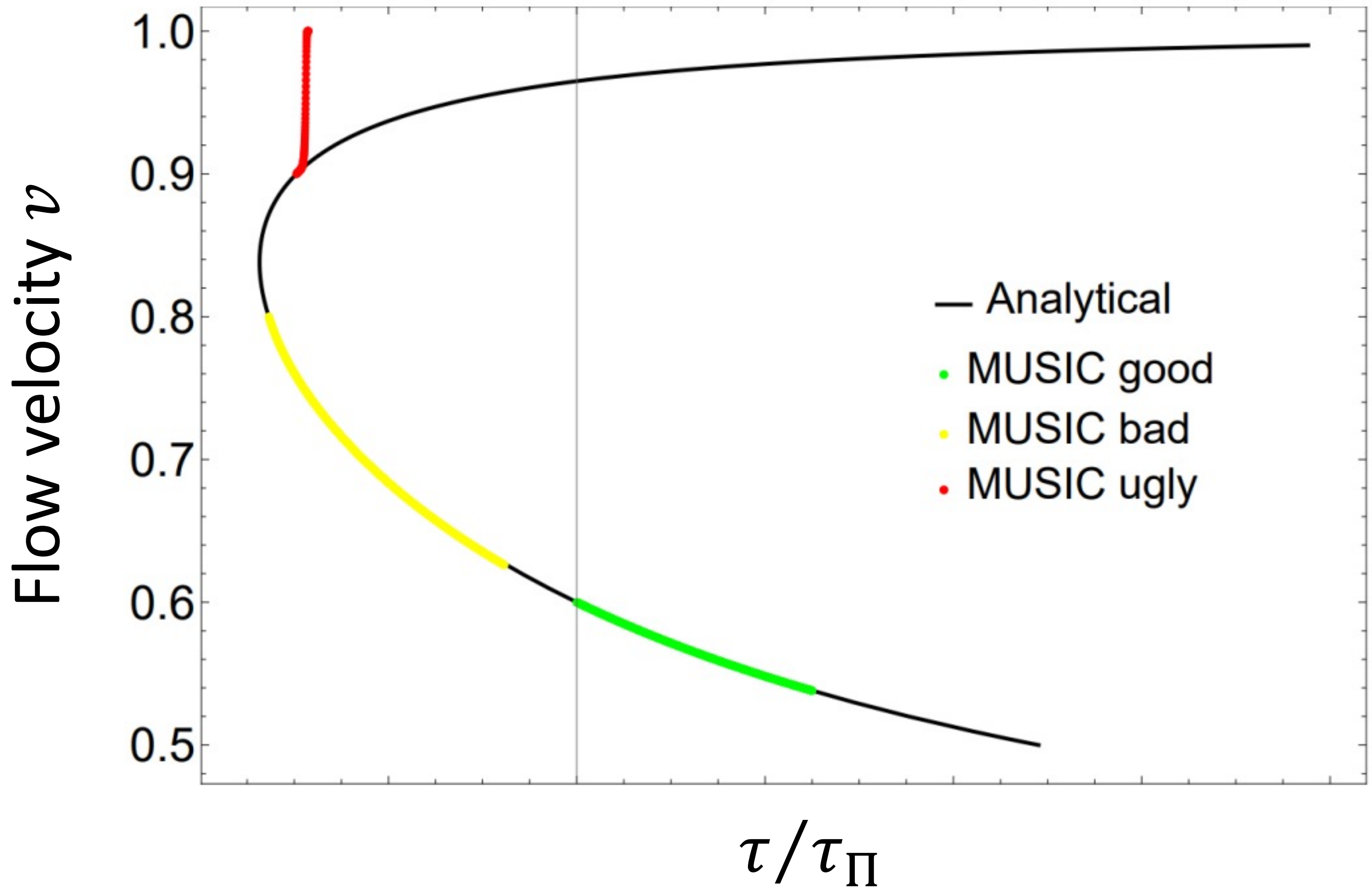

- Causality violations originate instabilities in the fluid description
- The codes do not see these instabilities

We are solving hydrodynamics beyond its applicable regime!

3D Bayesian analysis

Based on:

Andi Mankolli (parallel 6, Thu)

Thigao Siqueira Domingues (poster 2, Tue)

New constraints on model parameters

- Constraints from large and small, symmetric and asymmetric systems (Au+Au and d+Au)
- Constraints from wide range of measurements at forward/backward rapidities (global energy conservation)
- Constraints from causality in hydrodynamic simulations

New constraints on model parameters

- Constraints from large and small, symmetric and asymmetric systems (Au+Au and d+Au)
- Constraints from wide range of measurements at forward/backward rapidities (global energy conservation)
- Constraints from causality in hydrodynamic simulations

3D Initial State and Hydrodynamics

A. Mankolli

SOPHIA HADRON PHYSICS GROUP

Impose energy momentum conservation

α_{rem} (Remnant energy loss fraction)

Initial State

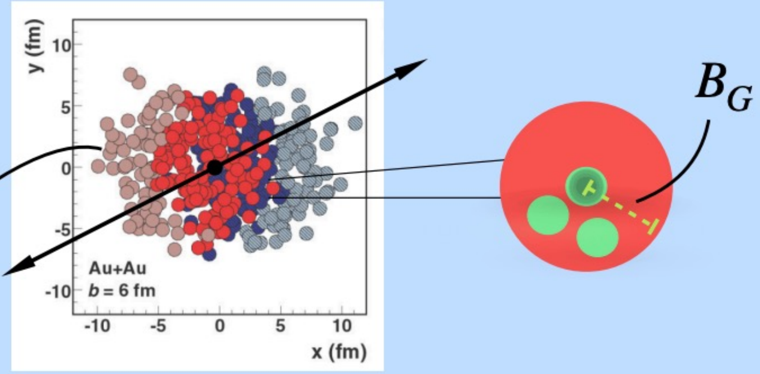

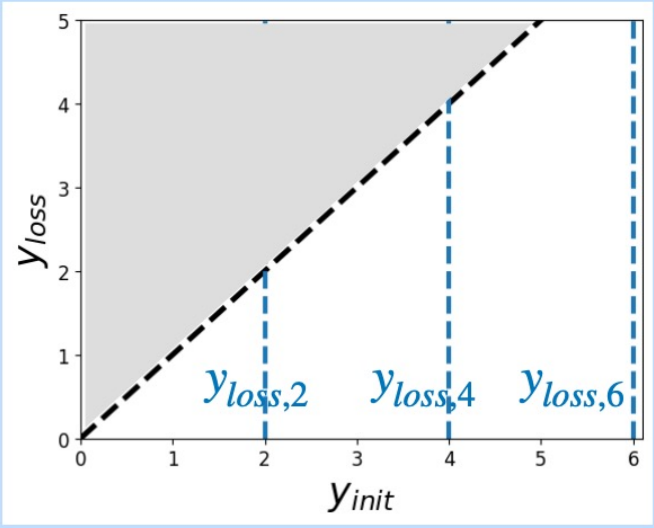

3D MCGlauber

Hydrodynamics

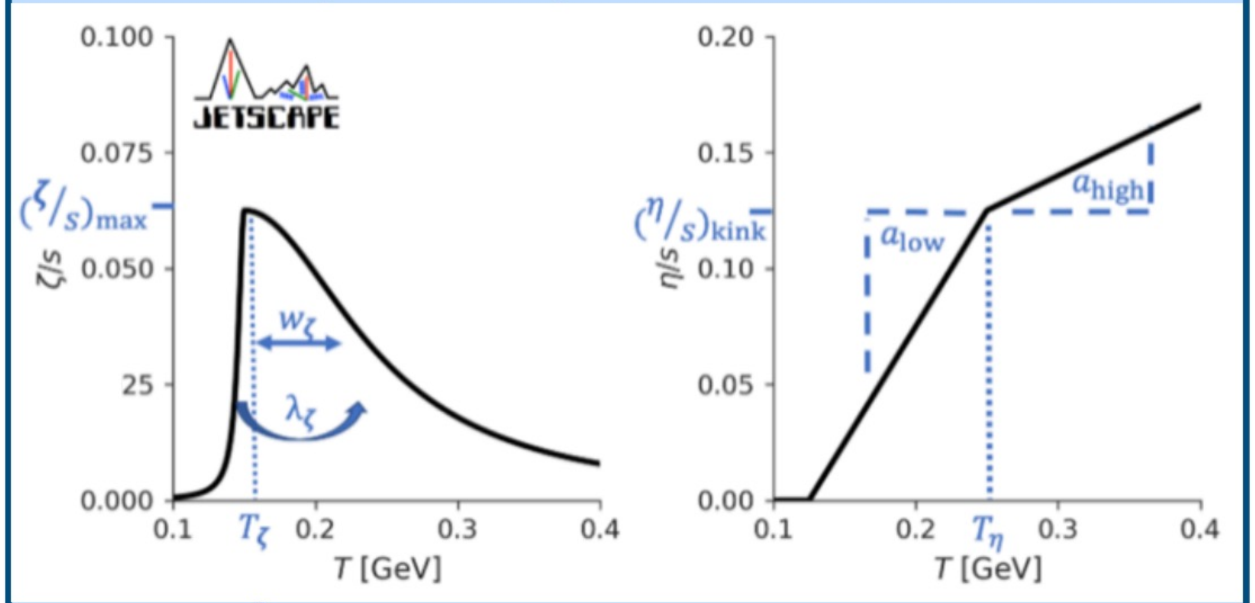

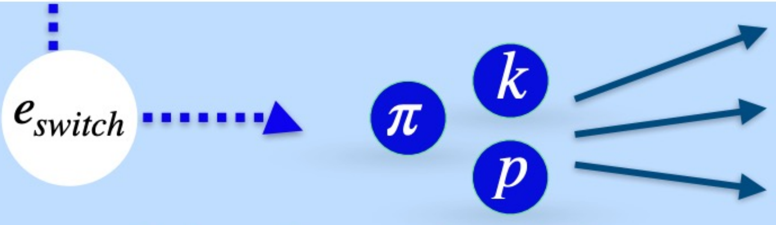

Hadronic Transport

MUSIC + UrQMD

Schenke, Shen, Zhao.

Phys. Rev. C 105, 064905 (2022)

Phys. Rev. C 97, 024907 (2018)

Calibrated model parameters

A. Mankolli

SOPHIA HADRON PHYSICS GROUP

Parameter	Collision Stage	Prior Range
$y_{loss,2}$	Initial State	[0,2]
$y_{loss,4}$	Initial State	[$y_{loss,2}$,4]
$y_{loss,6}$	Initial State	[$y_{loss,4}$,6]
$\sigma_{y_{loss}}$	Initial State	[0,1]
α_{rem}	Initial State	[0,1]
Shadowing Factor	Initial State	[0,1]
τ_{form} Mean	Initial State	[0.2,1]
B_G [1/GeV^2]	Initial State	[2,25]
String Source σ_x [fm]	Initial State	[0.1,0.5]
String Source σ_η	Initial State	[0.1,0.8]
String Trans. Shift Frac.	Initial State	[0,1]
$\frac{\eta}{s}$ T_{kink} [GeV]	Hydro	[0.13,0.3]
$\frac{\eta}{s}$ low-T slope	Hydro	[-2,1]
$\frac{\eta}{s}$ high-T slope	Hydro	[-1,2]
$\frac{\eta}{s}$ at kink	Hydro	[0.01,0.2]
$\frac{\zeta}{s}$ max	Hydro	[0.01,0.2]
$\frac{\zeta}{s}$ T_{peak} [GeV]	Hydro	[0.12,0.3]
$\frac{\zeta}{s}$ width	Hydro	[0.025,0.15]
$\frac{\zeta}{s}$ λ assym.	Hydro	[-0.8,0.6]
EPS Switch [GeV/fm^3]	Particlization	[0.1,0.6]

- 11 parameters for initial state
- 8 parameters for viscosities
- 1 parameter for particlization

Experimental data

A. Mankolli

SOPHIA HADRON PHYSICS GROUP

Au-Au 200 GeV

- $v_2(\eta)$ STAR
- $v_2(\eta)$ PHOBOS
- $\langle p_T \rangle$ π, k STAR
- $\langle p_T \rangle$ k, p PHENIX
- $\langle p_T \rangle$ p STAR
- $\langle p_T \rangle$ π PHENIX

- $dN_{ch}/d\eta(\eta)$ PHOBOS
- v_2(cent) STAR
- v_3(cent) STAR
- $v_2(p_T)$ PHENIX
- $v_2(p_T)$ STAR
- $v_3(p_T)$ PHENIX
- $v_4(p_T)$ PHENIX

- $dN_{ch}/d\eta(\eta)$ BRAHMS
- $r_2(\eta)$ STAR
- $r_3(\eta)$ STAR
- $dE_T/d\eta$(cent) PHENIX

d-Au 200 GeV

- $dN_{ch}/d\eta(\eta)$ PHOBOS
- $dN_{ch}/d\eta(\eta)$ PHENIX
- $v_2(p_T)$ PHENIX
- $v_2(p_T)$ STAR
- $v_2(\eta)$ PHENIX
- $v_3(p_T)$ STAR
- $v_3(p_T)$ PHENIX
- $dE_T/d\eta$(cent) PHENIX

Observables from calibrated model

A. Mankolli

SOPHIA HADRON PHYSICS GROUP

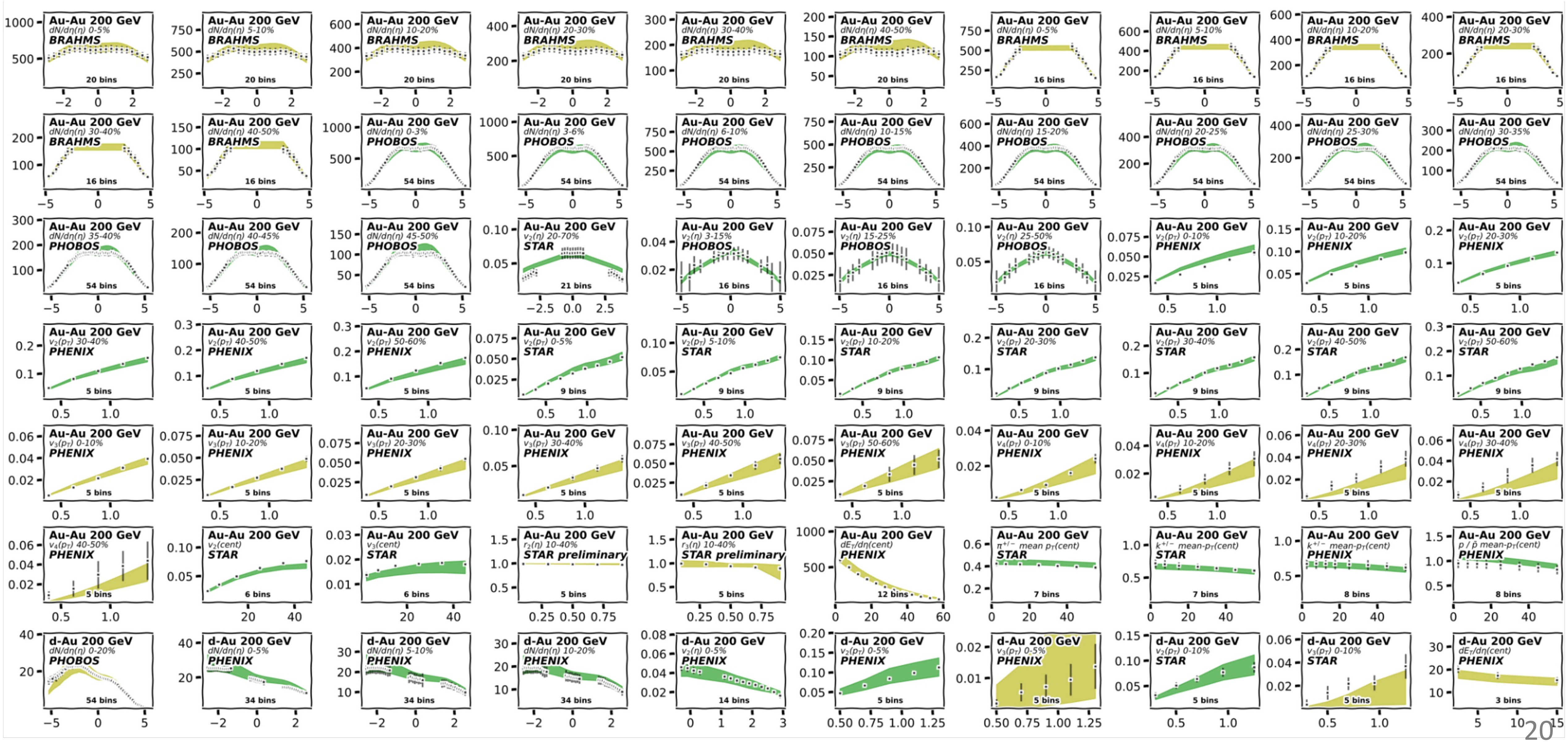

Observables from calibrated model

A. Mankolli

SOPHIA
HADRON
PHYSICS
GROUP

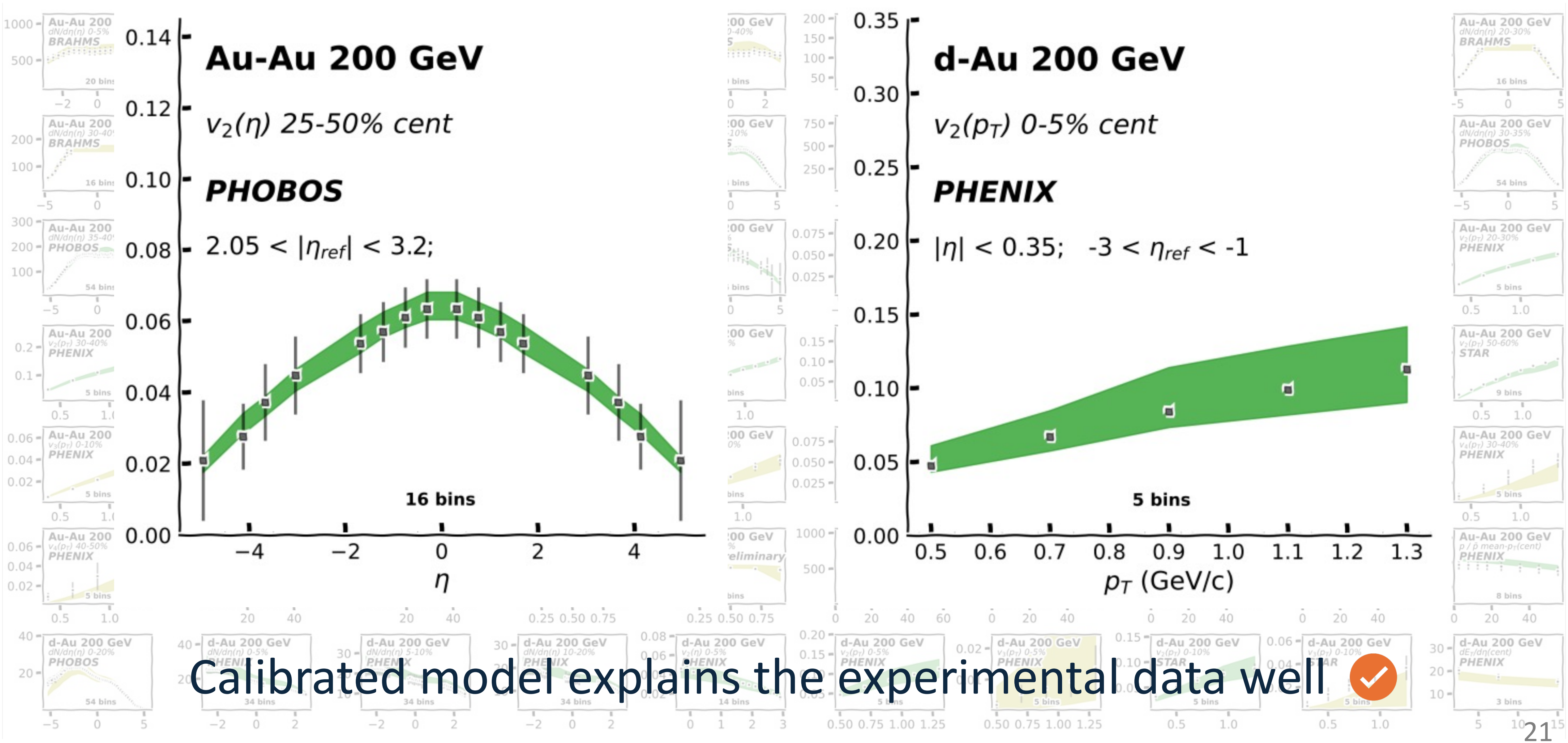

Calibrated model explains the experimental data well

Constraints from forward/backward

A. Mankolli

SOPHIA HADRON PHYSICS GROUP

Initial State

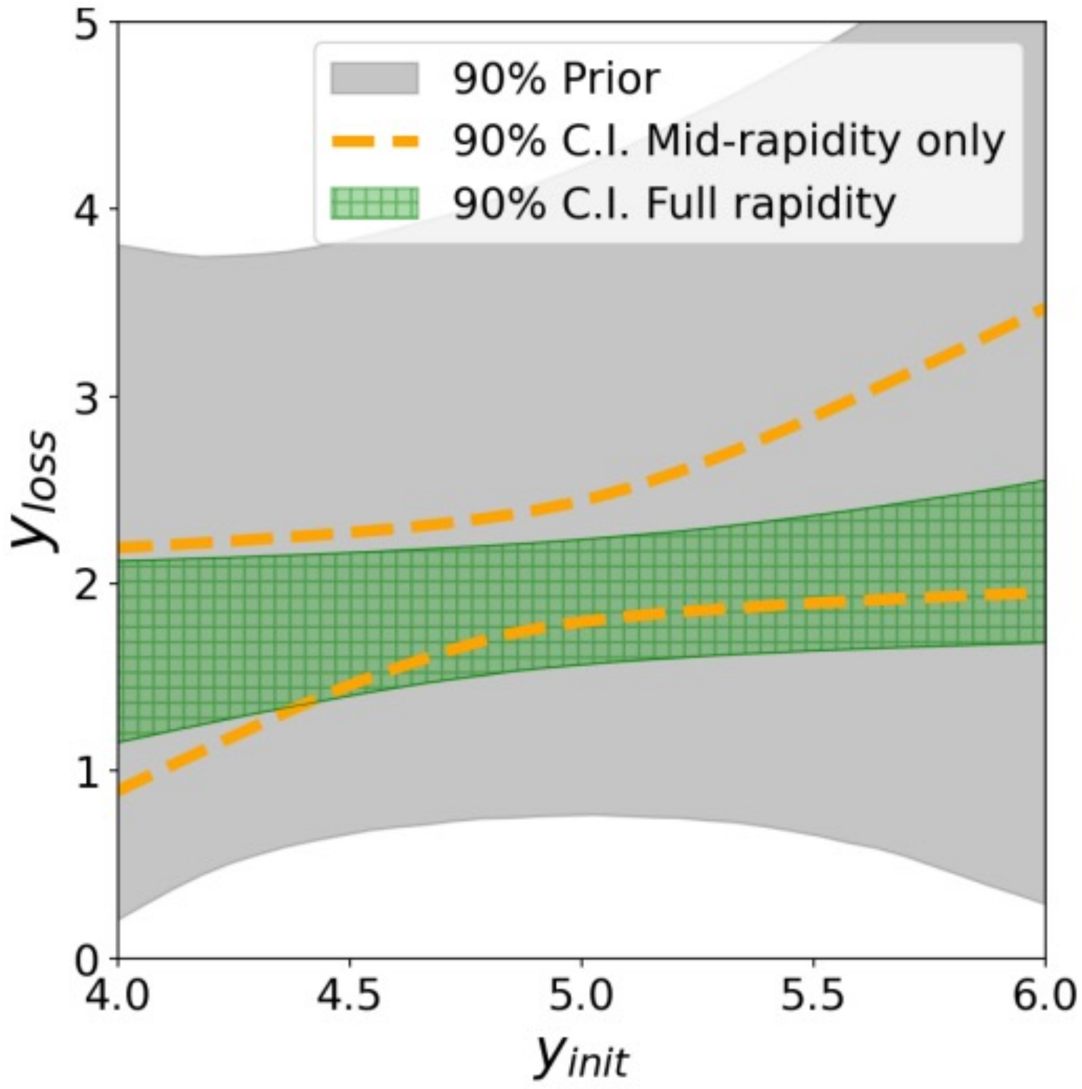

- The strongest constraint in the beam rapidity region,

$$y_{\mathrm{beam}}(\sqrt{s_{\mathrm{NN}}} = 200\ \mathrm{GeV}) = 5.36$$

- Significant rapidity loss constraints provided by midrapidity data
- Rapidity loss becomes less sensitive to y_{init} when forward/backward data is used

Constraints from forward/backward

A. Mankolli

SOPHIA HADRON PHYSICS GROUP

Viscosity

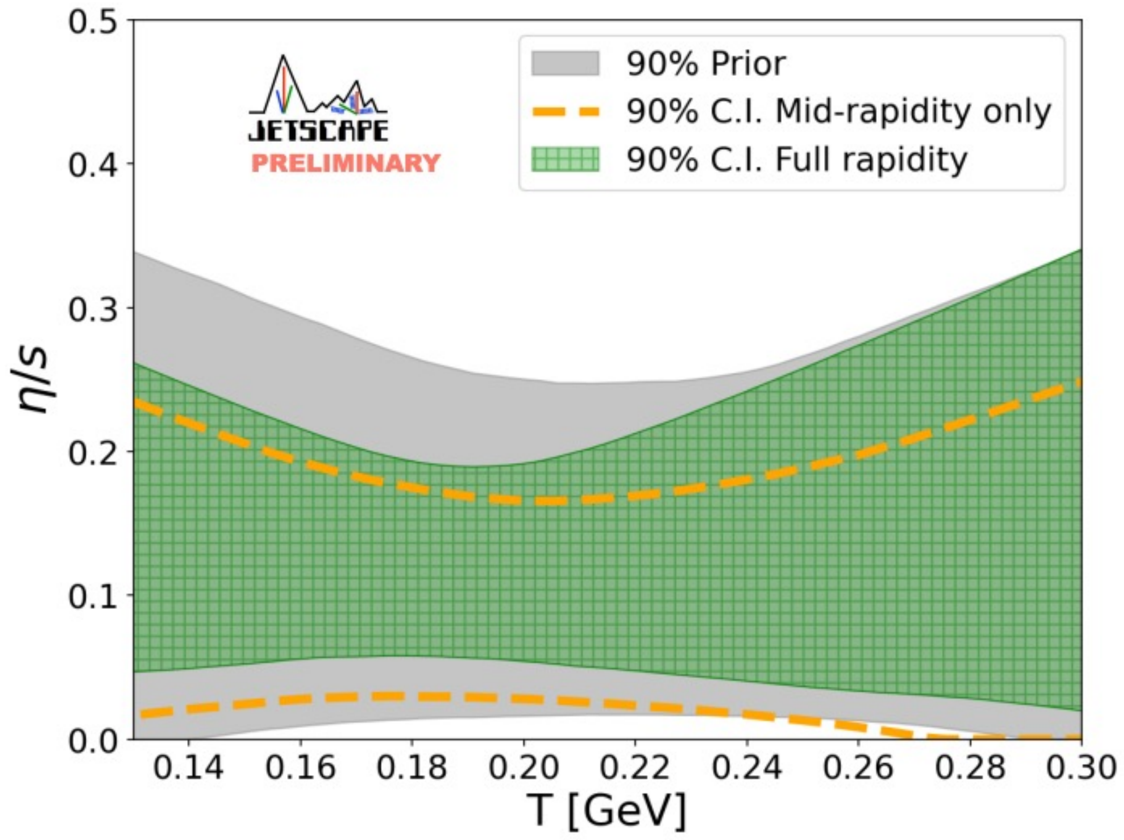

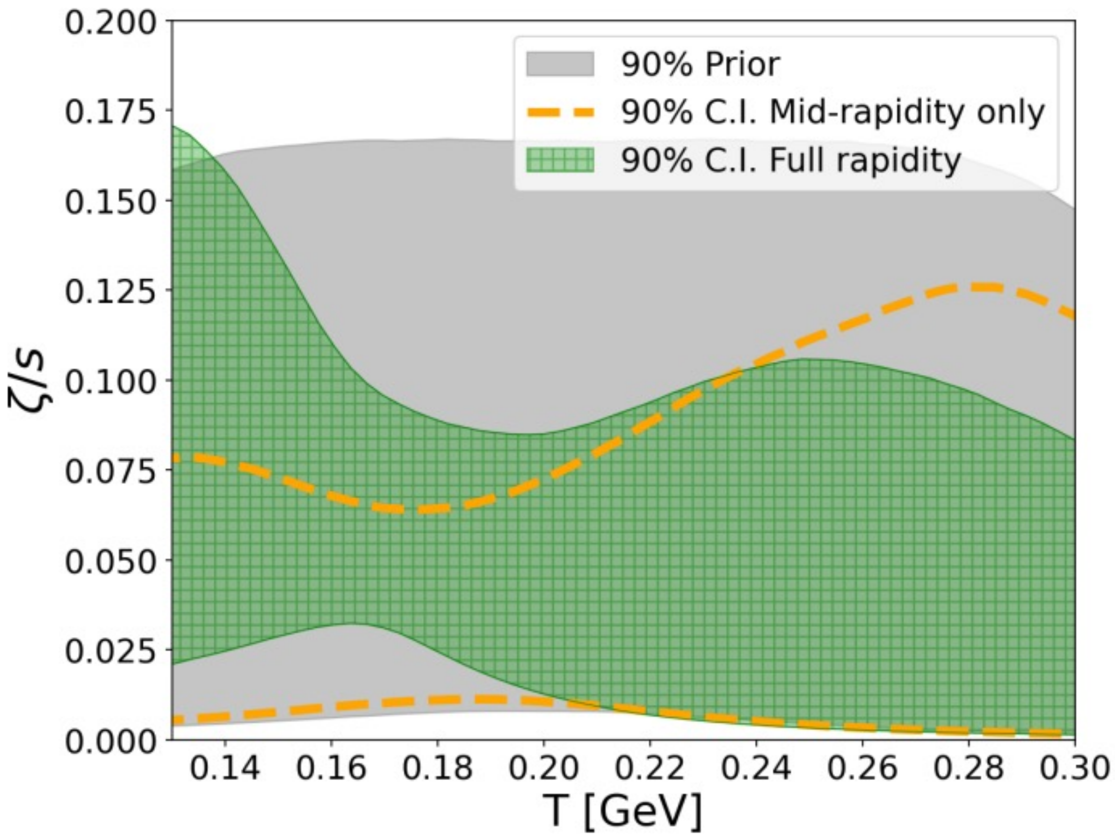

- Viscosity posteriors shifted to larger values
- Preference for finite bulk viscosity at low T

Constraints from different system

A. Mankolli

SOPHIA HADRON PHYSICS GROUP

Viscosity

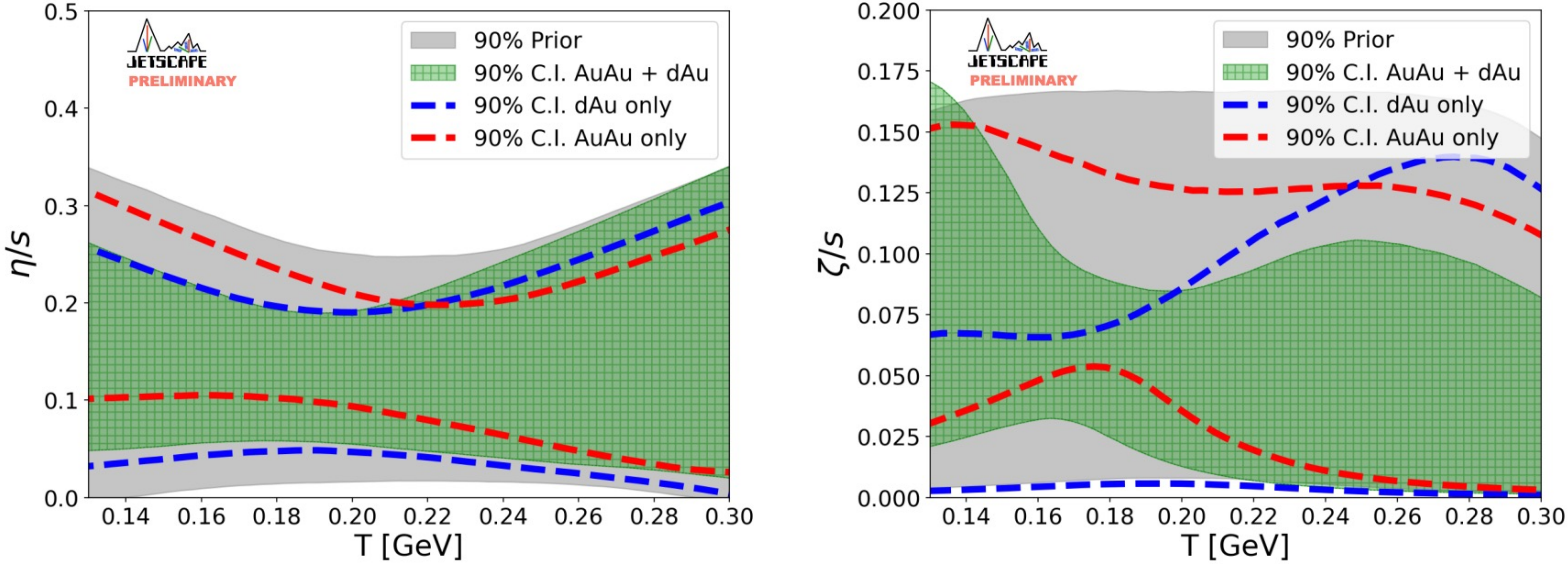

- Somewhat consistent individual system posteriors
- Stronger indication of finite viscosity from Au+Au

New constraints on model parameters

- Constraints from large and small, symmetric and asymmetric systems (Au+Au and d+Au)
- Constraints from wide range of measurements at forward/backward rapidities (global energy conservation)
- Constraints from causality in hydrodynamic simulations

3D dynamical model with causality

T. S. Domingues

SOPHIA HADRON PHYSICS GROUP

3D dynamical model

- T$_\mathrm{R}$ENTo [49] to generate the system's initial energy density;
- Free-streaming of the initial T$_\mathrm{R}$ENTo profile using [50];
- Viscous hydrodynamic evolution using the MUSIC code [51];
- Particlization based on the Cooper-Frye formula using the frzout code [52];
- Boltzmann evolution and decays of hadrons using the UrQMD code [53].

Necessary conditions for causality

$$n_1 \equiv \frac{2}{C_\eta} + \frac{\lambda_{\pi\Pi}}{\tau_\pi}\frac{\Pi}{\varepsilon+P} - \frac{\tau_{\pi\pi}}{2\tau_\pi}\frac{|\Lambda_1|}{\varepsilon+P} \geq 0, \tag{8a}$$

$$n_2 \equiv 1 - \frac{1}{C_\eta} + \left(1 - \frac{\lambda_{\pi\Pi}}{2\tau_\pi}\right)\frac{\Pi}{\varepsilon+P} - \frac{\tau_{\pi\pi}}{4\tau_\pi}\frac{\Lambda_3}{\varepsilon+P} \geq 0, \tag{8b}$$

$$n_3 \equiv \frac{1}{C_\eta} + \frac{\lambda_{\pi\Pi}}{2\tau_\pi}\frac{\Pi}{\varepsilon+P} - \frac{\tau_{\pi\pi}}{4\tau_\pi}\frac{\Lambda_3}{\varepsilon+P} \geq 0, \tag{8c}$$

$$\begin{aligned} n_4 \equiv\ & 1 - \frac{1}{C_\eta} + \left(1 - \frac{\lambda_{\pi\Pi}}{2\tau_\pi}\right)\frac{\Pi}{\varepsilon+P} \\ & + \left(1 - \frac{\tau_{\pi\pi}}{4\tau_\pi}\right)\frac{\Lambda_a}{\varepsilon+P} - \frac{\tau_{\pi\pi}}{4\tau_\pi}\frac{\Lambda_d}{\varepsilon+P} \geq 0,\ (a \neq d) \end{aligned} \tag{8d}$$

$$\begin{aligned} n_5 \equiv\ & c_s^2 + \frac{4}{3}\frac{1}{C_\eta} + \frac{1}{C_\zeta} + \left(\frac{2}{3}\frac{\lambda_{\pi\Pi}}{\tau_\pi} + \frac{\delta_{\Pi\Pi}}{\tau_\Pi} + c_s^2\right)\frac{\Pi}{\varepsilon+P} \\ & + \left(\frac{3\delta_{\pi\pi}+\tau_{\pi\pi}}{3\tau_\pi} + \frac{\lambda_{\Pi\pi}}{\tau_\Pi} + c_s^2\right)\frac{\Lambda_1}{\varepsilon+P} \geq 0, \end{aligned} \tag{8e}$$

$$\begin{aligned} {}_6 \equiv\ & 1 - \left(c_s^2 + \frac{4}{3}\frac{1}{C_\eta} + \frac{1}{C_\zeta}\right) \\ & + \left(1 - \frac{2}{3}\frac{\lambda_{\pi\Pi}}{\tau_\pi} - \frac{\delta_{\Pi\Pi}}{\tau_\Pi} - c_s^2\right)\frac{\Pi}{\varepsilon+P} \\ & + \left(1 - \frac{3\delta_{\pi\pi}+\tau_{\pi\pi}}{3\tau_\pi} - \frac{\lambda_{\Pi\pi}}{\tau_\Pi} - c_s^2\right)\frac{\Lambda_3}{\varepsilon+P} \geq 0. \end{aligned} \tag{8f}$$

T. S. Domingues *et al.*, Phys. Rev. C **110**, 064904 (2024)

F. S. Bemfica *et al.*, Phys. Rev. Lett. **126**, 222301 (2021)

Impose causality constraint

T. S. Domingues

SOPHIA HADRON PHYSICS GROUP

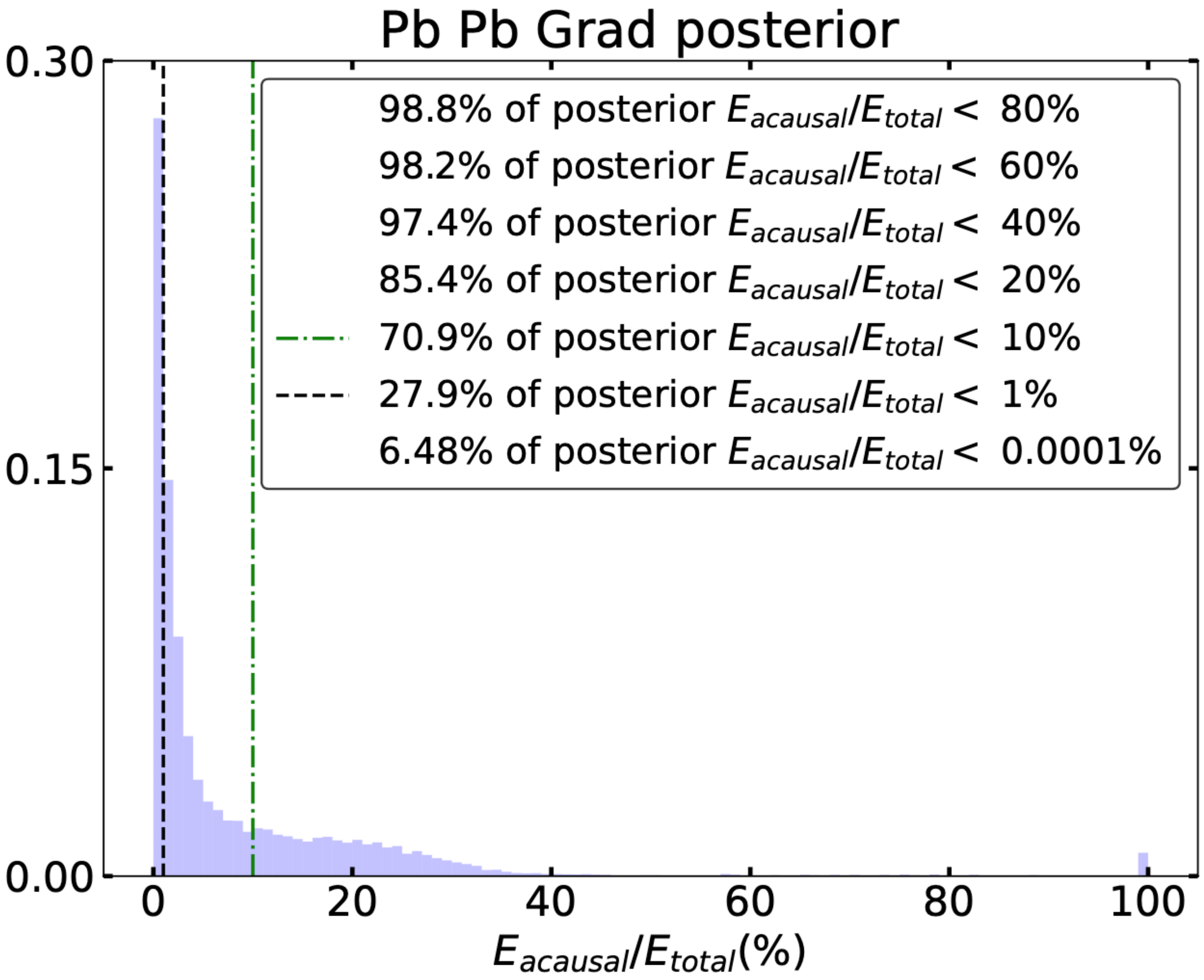

Acausality fraction $\frac{E_{\text{acausal}}}{E_{\text{total}}}$

E_{acausal}: energy in acausal region

E_{total}: Initial total energy

- Impose cutoffs for acausality fraction
- Constraints on prior from the causality

Posterior distributions of parameters

T. S. Domingues

SOPHIA HADRON PHYSICS GROUP

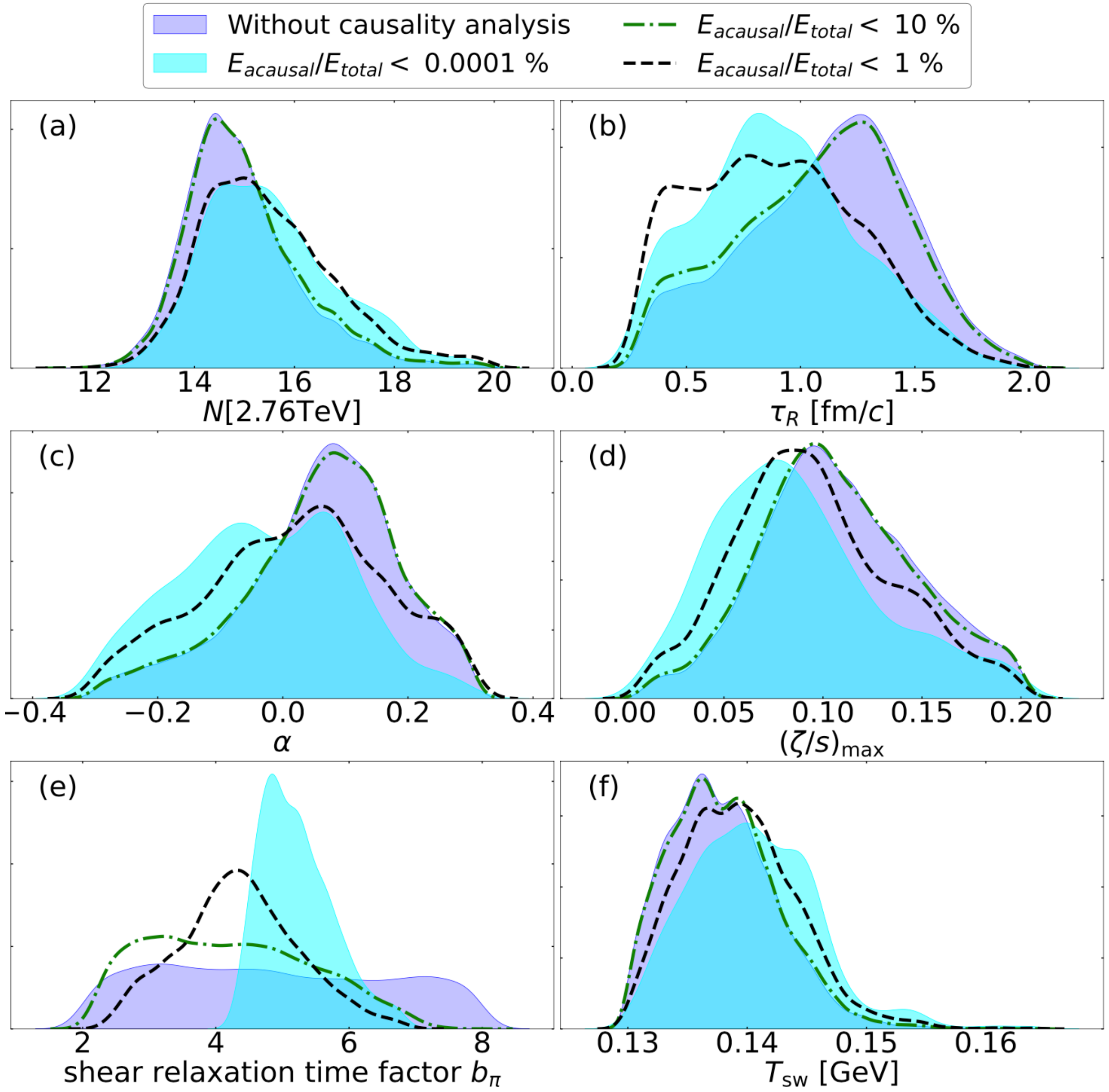

Initial Stage

$$\tau\epsilon(\mathbf{x}_\perp) = N\left(\frac{T_A^p(\mathbf{x}_\perp)+T_B^p(\mathbf{x}_\perp)}{2}\right)^{1/p} \qquad \tau_{\rm fs} = \tau_R\left(\frac{\langle\bar\epsilon\rangle}{\bar\epsilon_R}\right)^{\alpha}$$

Transport Coefficient

$$\frac{\zeta}{s}(T) = \frac{(\zeta/s)_{\max}\Lambda^2}{\Lambda^2+(T-T_\zeta)^2}, \qquad T\tau_\pi(T) = b_\pi\frac{\eta}{s}(T)$$

Particlization

T_{sw}: switching temperature

Visible effects from causality constraint!

Posterior distributions of viscosities

T. S. Domingues

SOPHIA HADRON PHYSICS GROUP

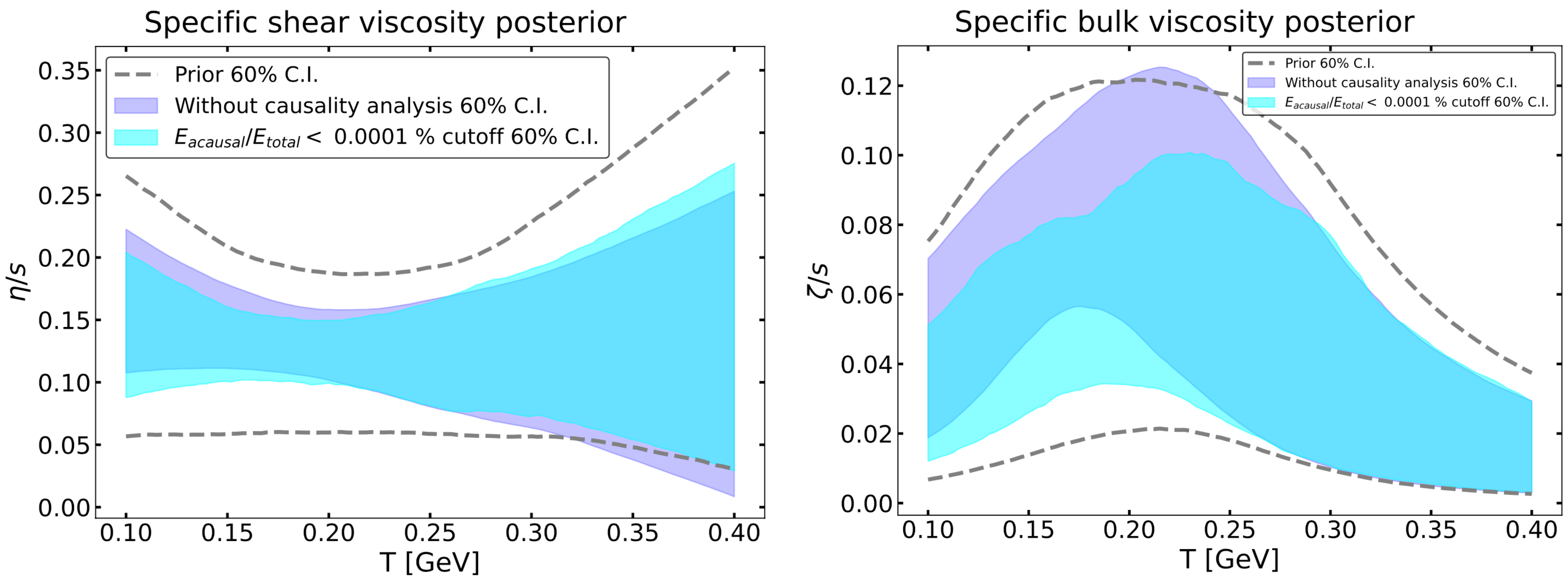

- Visible effects on viscosities from causality analysis
- Preference for small shear and bulk viscosities at low T

Observable posterior

T. S. Domingues

SOPHIA HADRON PHYSICS GROUP

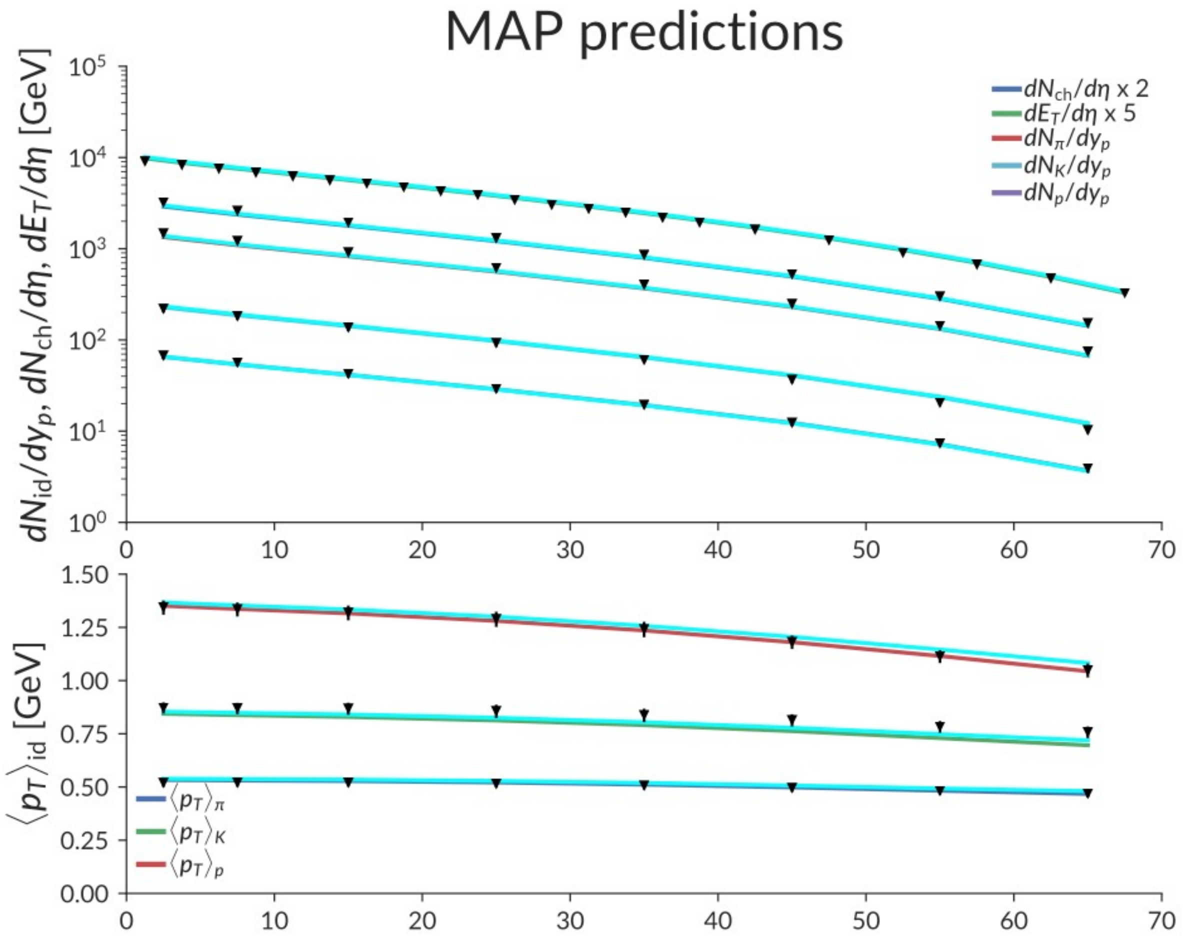

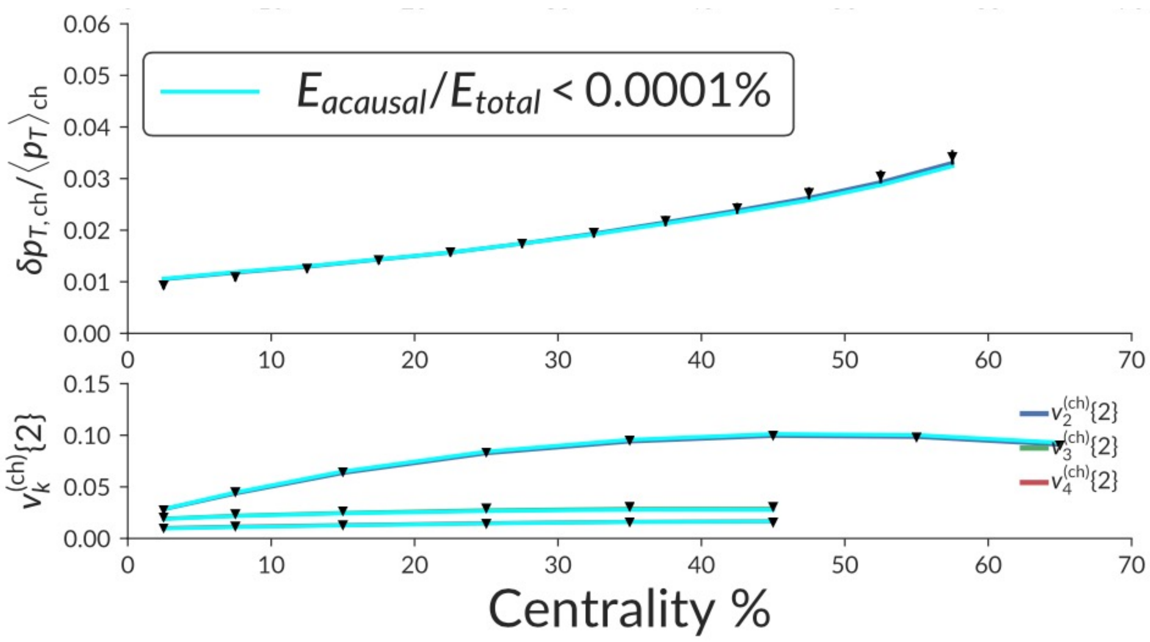

- Even after imposing causality cutoff, there is no discrepancy with unconstrained posterior

Nuclear structure in high-energy collisions

Based on:
Chun Shen (parallel 22, Tue)
Govert Nijs (plenary 6, Thu)

Nuclear deformation

C. Shen

The ground state configurations of heavy nuclei can be described by generalized Woods-Saxon profile with intrinsic deformations:

$$\rho(r,\theta,\phi) = \frac{\rho_0}{1+\exp\left[\left(r-R(\theta,\phi)\right)/a_0\right]}$$

$$R(\theta,\phi) = R_0\left[1+\beta_2\left(\cos\gamma\, Y_{2,0}(\theta,\phi)+\sin\gamma\, Y_{2,2}(\theta,\phi)\right)+\beta_3 Y_{3,0}(\theta,\phi)+\beta_4 Y_{4,0}(\theta,\phi)\right]$$

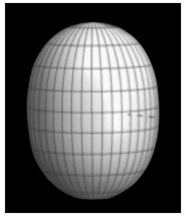

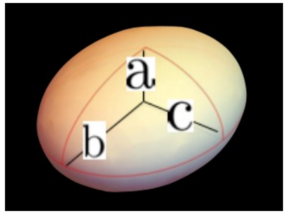

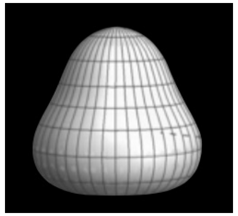

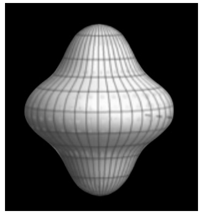

- Intrinsic shapes encode multi-particle correlations that are probed by heavy-ion observables
- Observable ratios $\frac{\mathcal{O}_{\mathrm{X+X}}}{\mathcal{O}_{\mathrm{y+y}}}$ cancel effects from QGP evolution

Imaging nuclear shapes

SOPHIA HADRON PHYSICS GROUP

- Nuclear deformation

RHIC

$$\frac{\mathcal{O}_{\mathrm{Ru+Ru}}}{\mathcal{O}_{\mathrm{Zr+Zr}}} \qquad \frac{\mathcal{O}_{\mathrm{U+U}}}{\mathcal{O}_{\mathrm{Au+Au}}}$$

(backup)

LHC

$$\frac{\mathcal{O}_{\mathrm{Xe+Xe}}}{\mathcal{O}_{\mathrm{Pb+Pb}}}$$

- Nuclear structure of light nuclei $^{16}\mathrm{O}$

$$\mathcal{O}_{\mathrm{O+O}}$$

(backup)

$$\mathcal{O}_{\mathrm{O+O}} \qquad \frac{\mathcal{O}_{\mathrm{O+O}}}{\mathcal{O}_{\mathrm{Pb+Pb}}}$$

- The nuclear bowling pin $^{20}\mathrm{Ne}$

$$\frac{\mathcal{O}_{\mathrm{Ne+Ne}}}{\mathcal{O}_{\mathrm{O+O}}} \qquad \frac{\mathcal{O}_{\mathrm{Ne+Pb}}}{\mathcal{O}_{\mathrm{O+Pb}}}$$

Predictions only

Constraining nuclear deformation

C. Shen

SOPHIA HADRON PHYSICS GROUP

^{238}U vs. ^{197}Au

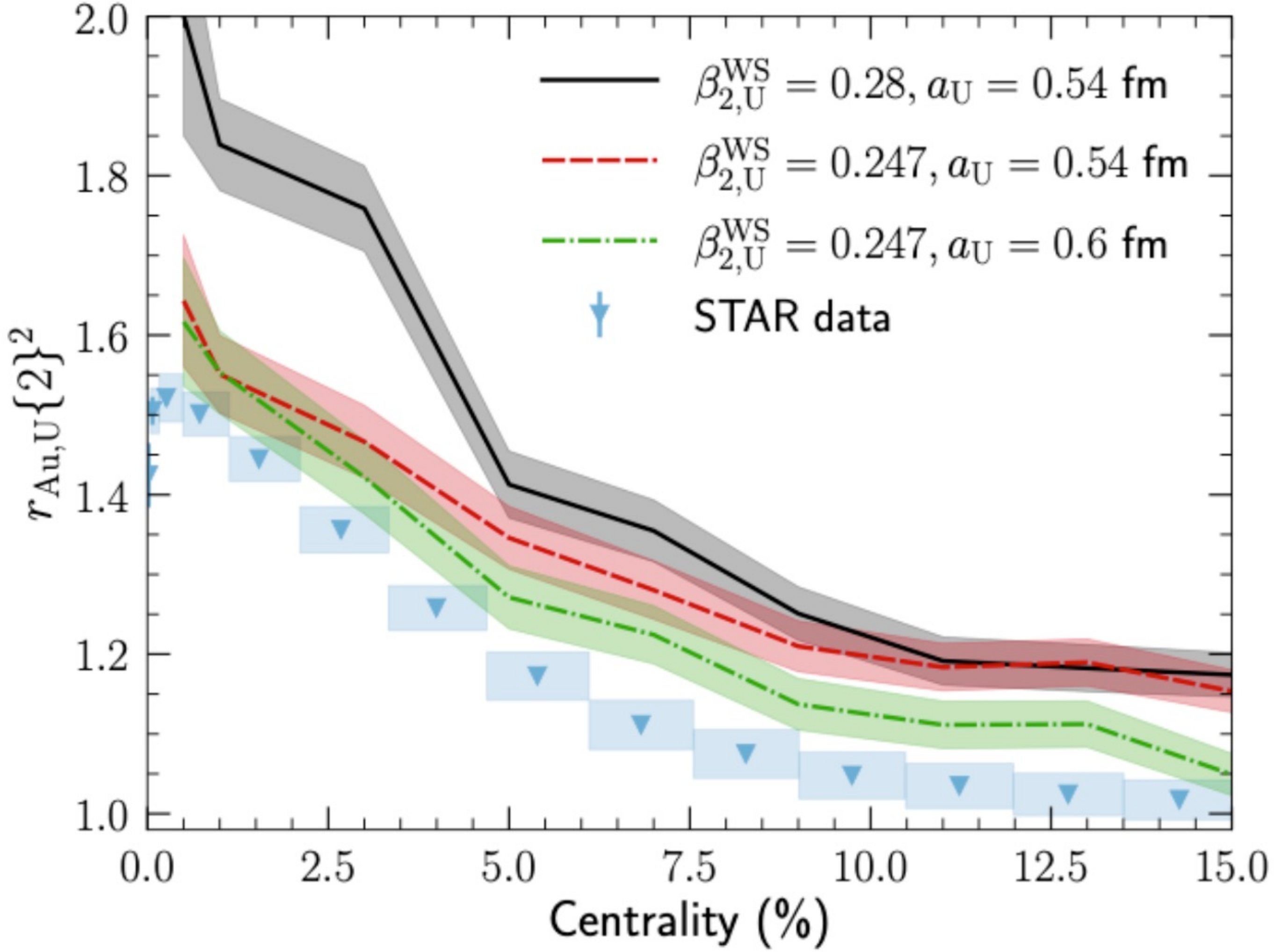

$$r^2_{\mathrm{Au,U}}\{2\} = \frac{v_2^{\mathrm{U}}\{2\}^2}{v_2^{\mathrm{Au}}\{2\}^2}$$

^{197}Au ^{238}U

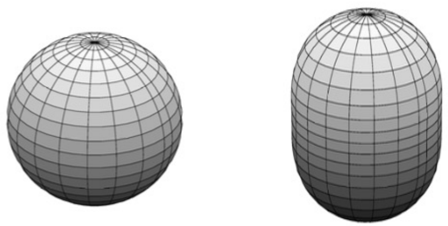

The ratio of elliptic flow in central U+U and Au+Au favors

$$\beta_{2,\mathrm{U}} = 0.247$$

$$a_{\mathrm{U}} = 0.6 \text{ fm}$$

W. Ryssens, G. Giacalone, B. Schenke and C. Shen, Phys. Rev. Lett. **130**, 212302 (2023)

Nuclear deformation of ^{129}Xe

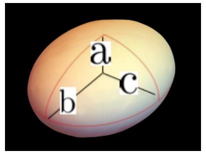

C. Shen

SOPHIA HADRON PHYSICS GROUP

^{129}Xe vs. ^{208}Pb

H. Mantysaari, B. Schenke, C. Shen and W. Zhao, Phys. Rev. C110, 054913 (2024)

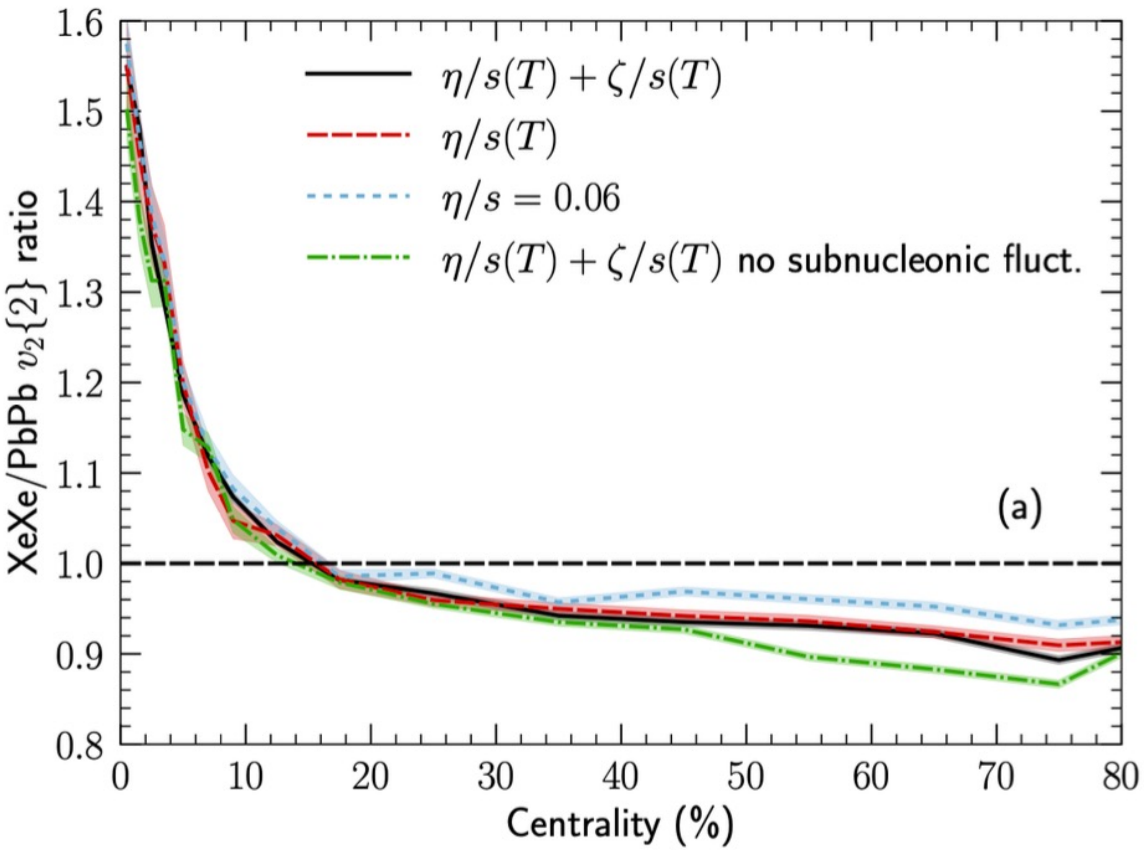

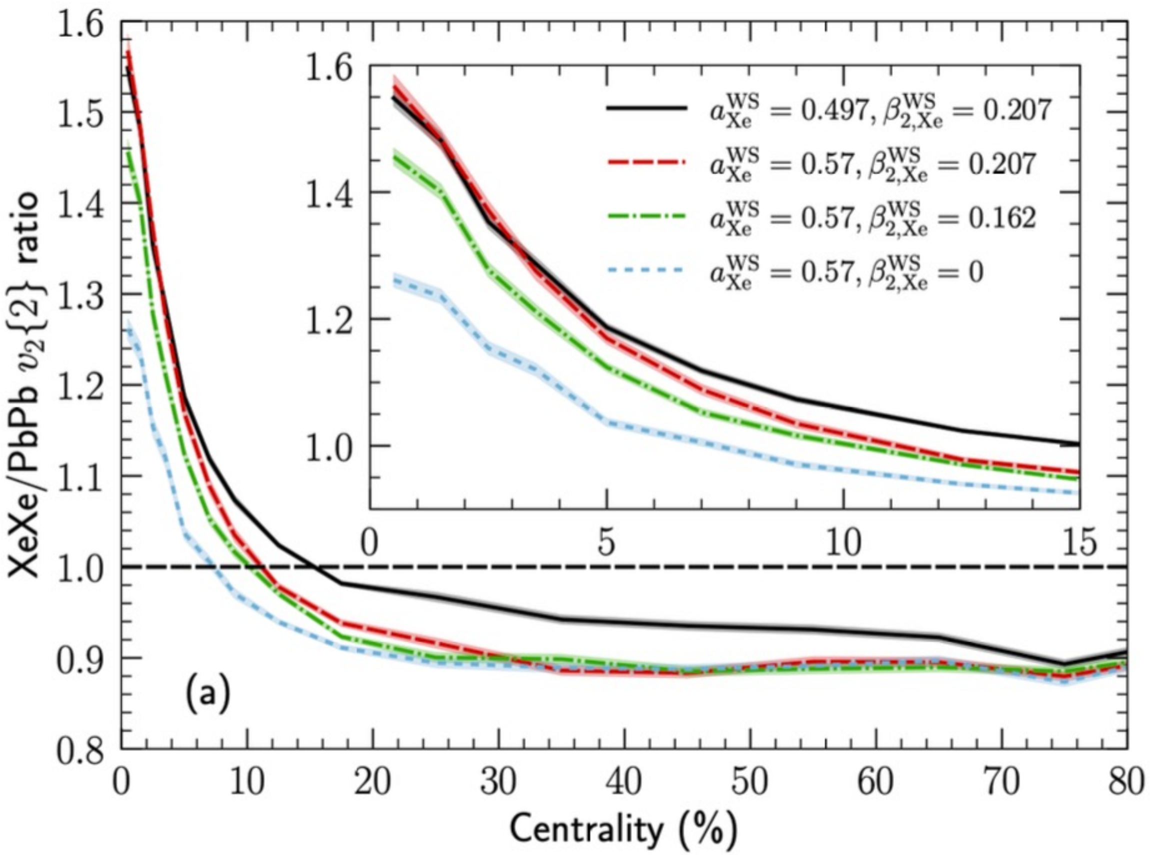

- No sensitivity to hydrodynamic evolution (viscosities)
- Strong sensitivity to the β_2 deformation

Nuclear deformation of ^{129}Xe

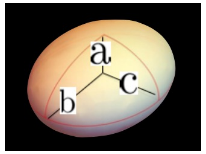

C. Shen

SOPHIA HADRON PHYSICS GROUP

^{129}Xe vs. ^{208}Pb

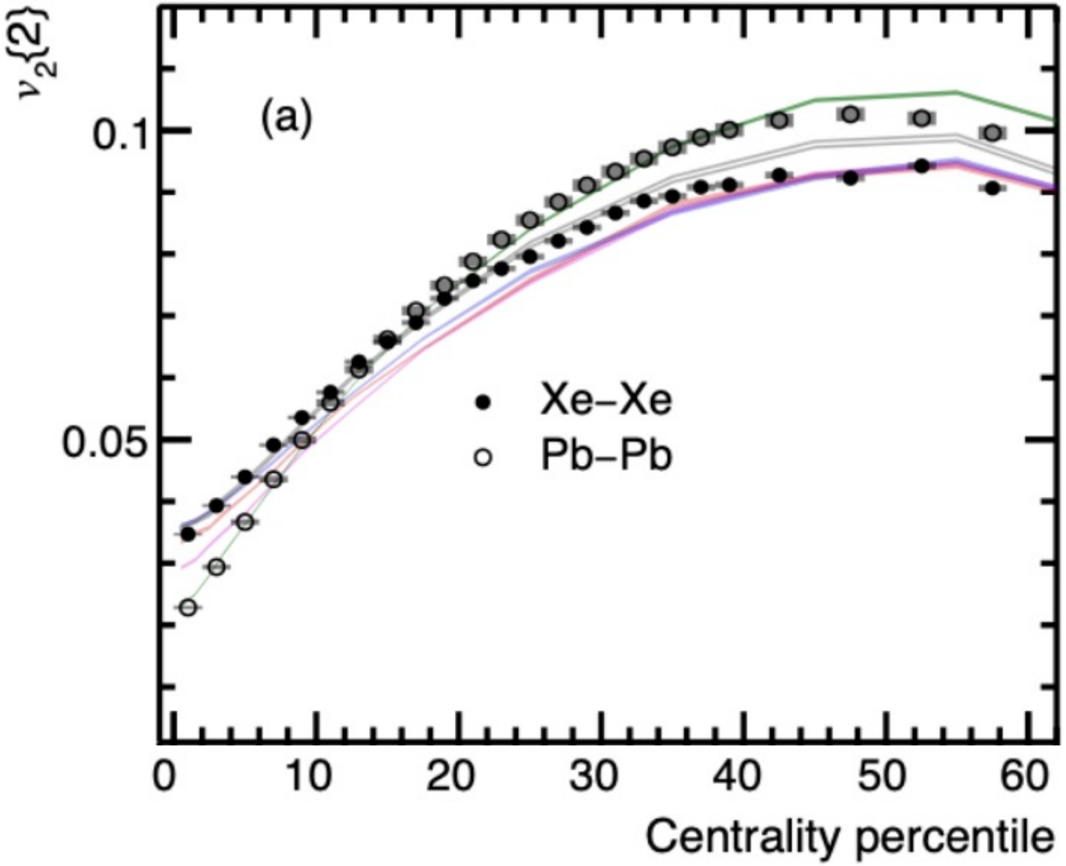

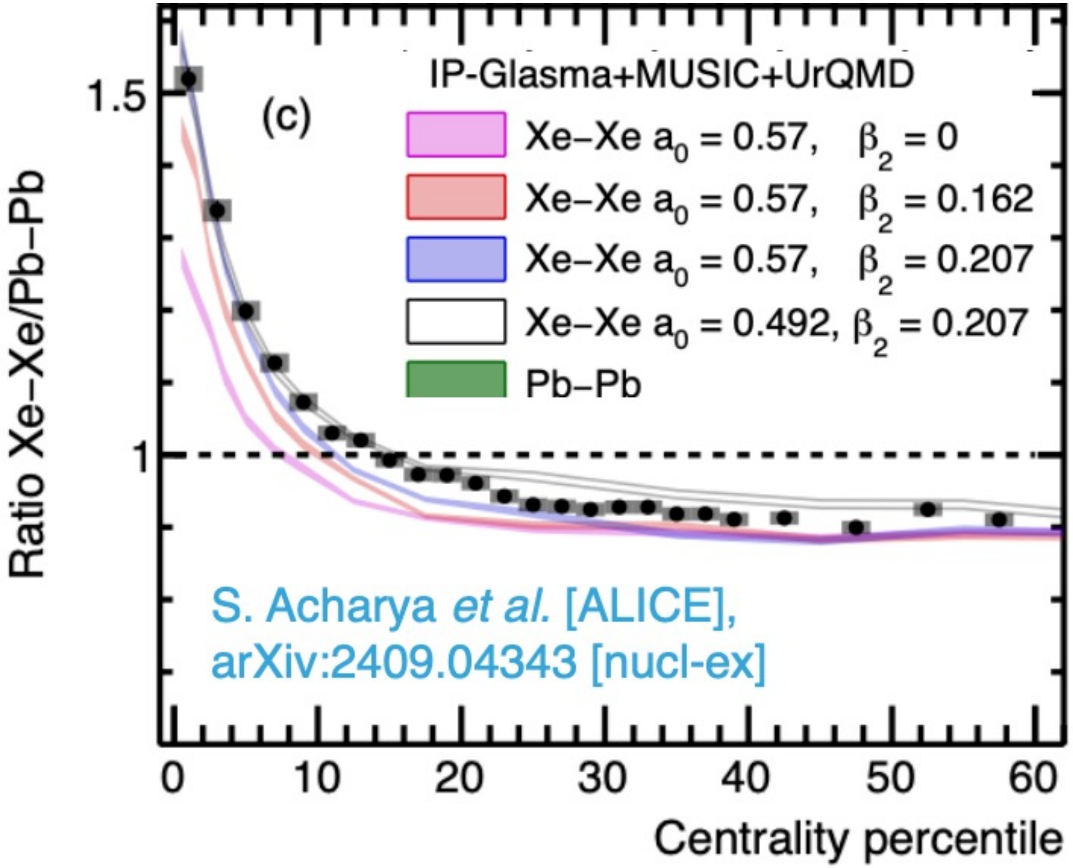

- Dynamical model explains the experimental data well

Imaging nuclear shapes

SOPHIA HADRON PHYSICS GROUP

- Nuclear deformation

RHIC

$$\frac{\mathcal{O}_{\mathrm{Ru+Ru}}}{\mathcal{O}_{\mathrm{Zr+Zr}}} \qquad \frac{\mathcal{O}_{\mathrm{U+U}}}{\mathcal{O}_{\mathrm{Au+Au}}}$$

(backup)

LHC

$$\frac{\mathcal{O}_{\mathrm{Xe+Xe}}}{\mathcal{O}_{\mathrm{Pb+Pb}}}$$

- Nuclear structure of light nuclei $^{16}\mathrm{O}$

$$\mathcal{O}_{\mathrm{O+O}}$$

(backup)

$$\mathcal{O}_{\mathrm{O+O}} \qquad \frac{\mathcal{O}_{\mathrm{O+O}}}{\mathcal{O}_{\mathrm{Pb+Pb}}}$$

- The nuclear bowling pin $^{20}\mathrm{Ne}$

$$\frac{\mathcal{O}_{\mathrm{Ne+Ne}}}{\mathcal{O}_{\mathrm{O+O}}} \qquad \frac{\mathcal{O}_{\mathrm{Ne+Pb}}}{\mathcal{O}_{\mathrm{O+Pb}}}$$

Predictions only

Predictions for $^{16}\mathrm{O} + {}^{16}\mathrm{O}$ at the LHC

G. Nijs

SOPHIA HADRON PHYSICS GROUP

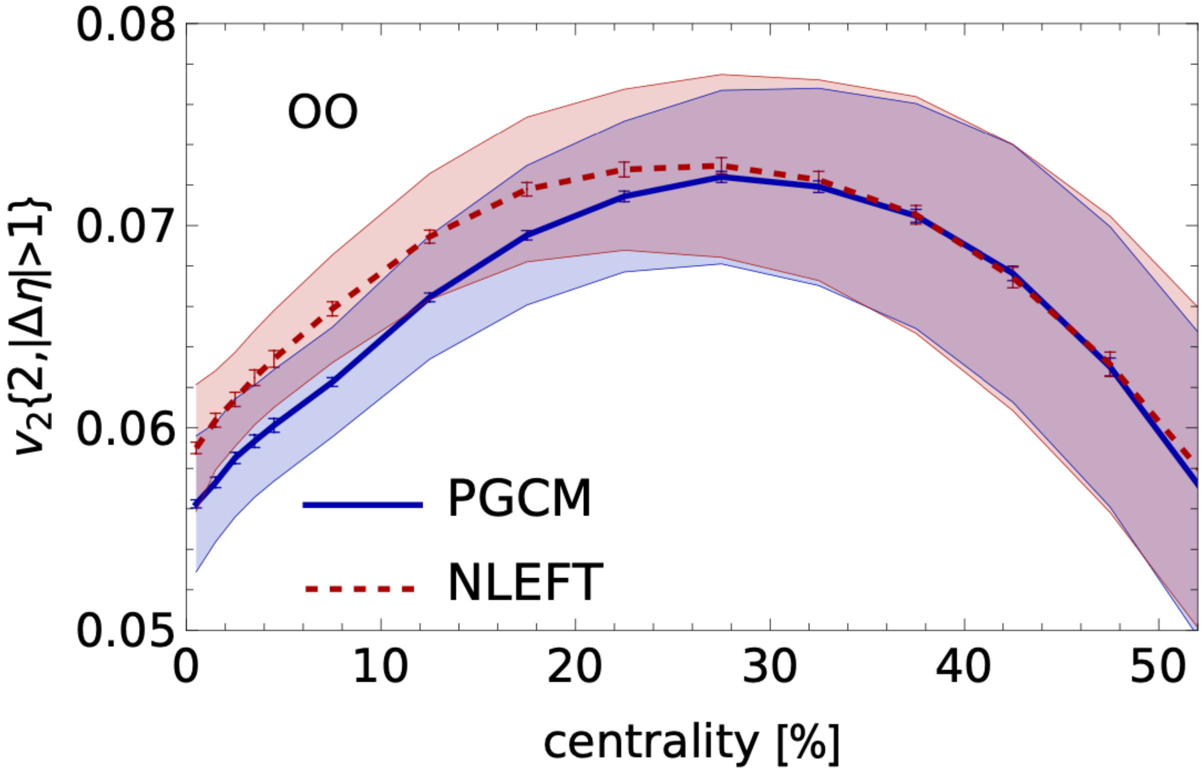

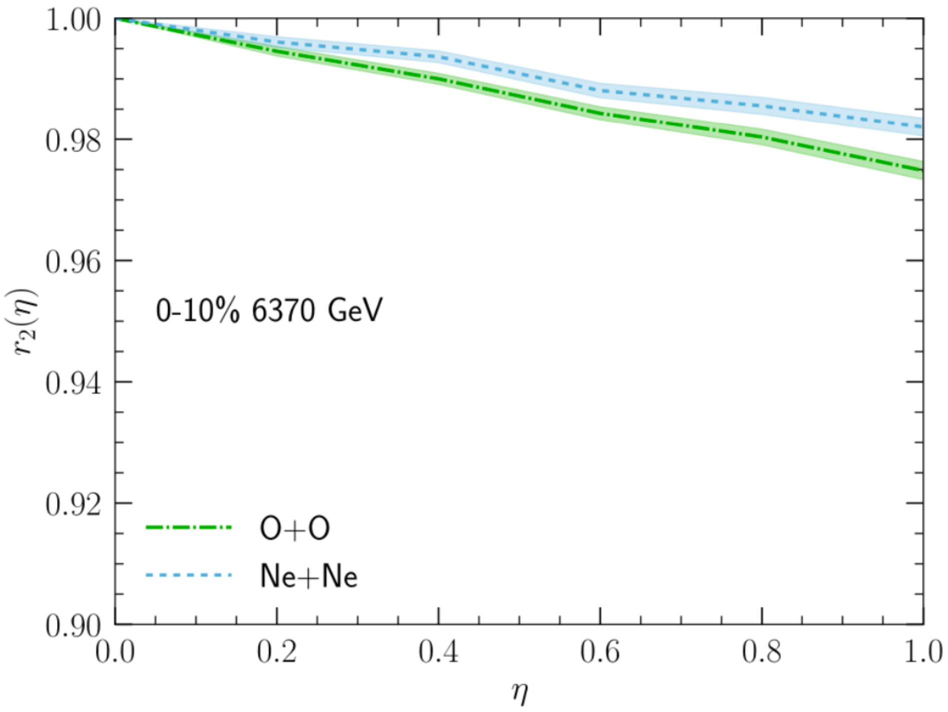

- Predictions using the parameters obtained by Bayesian analysis
- Different nuclear structure models give slightly different but consistent answers

Predictions for $^{16}\mathrm{O} + {}^{16}\mathrm{O}$ at the LHC

C. Shen

SOPHIA HADRON PHYSICS GROUP

$^{16}\mathrm{O}$ vs. $^{208}\mathrm{Pb}$

H. Mantysaari, B. Schenke, C. Shen and W. Zhao, Phys. Rev. C110, 054913 (2024)

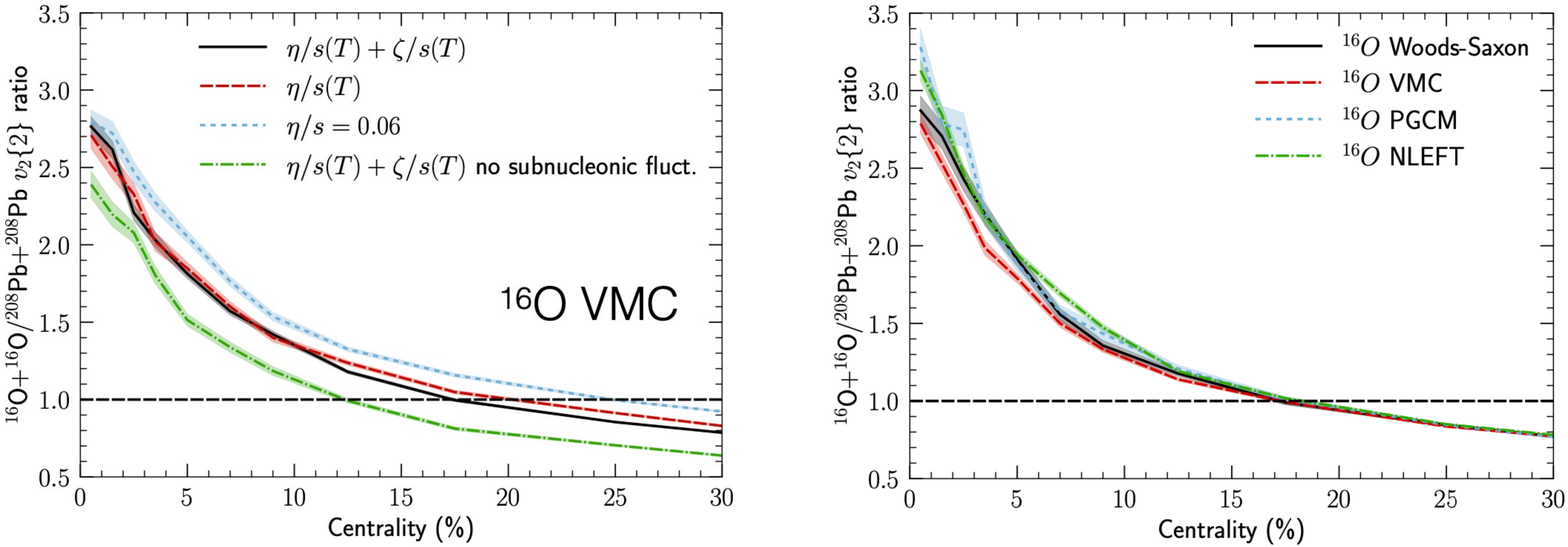

- Little sensitivity to hydrodynamic evolution
- Sizeable sensitivity to the sub-nucleonic fluctuations and structure

Imaging nuclear shapes

- Nuclear deformation

RHIC

$$\frac{\mathcal{O}_{\mathrm{Ru+Ru}}}{\mathcal{O}_{\mathrm{Zr+Zr}}} \qquad \frac{\mathcal{O}_{\mathrm{U+U}}}{\mathcal{O}_{\mathrm{Au+Au}}}$$

(backup)

LHC

$$\frac{\mathcal{O}_{\mathrm{Xe+Xe}}}{\mathcal{O}_{\mathrm{Pb+Pb}}}$$

- Nuclear structure of light nuclei $^{16}\mathrm{O}$

$$\mathcal{O}_{\mathrm{O+O}}$$

(backup)

$$\mathcal{O}_{\mathrm{O+O}} \qquad \frac{\mathcal{O}_{\mathrm{O+O}}}{\mathcal{O}_{\mathrm{Pb+Pb}}}$$

- The nuclear bowling pin $^{20}\mathrm{Ne}$

$$\frac{\mathcal{O}_{\mathrm{Ne+Ne}}}{\mathcal{O}_{\mathrm{O+O}}} \qquad \frac{\mathcal{O}_{\mathrm{Ne+Pb}}}{\mathcal{O}_{\mathrm{O+Pb}}}$$

Predictions only

The nuclear bowling pin ^{20}Ne

G. Nijs

SOPHIA HADRON PHYSICS GROUP

Giacalone, Bally, Nijs, Shen *et al.*, 2402.05995

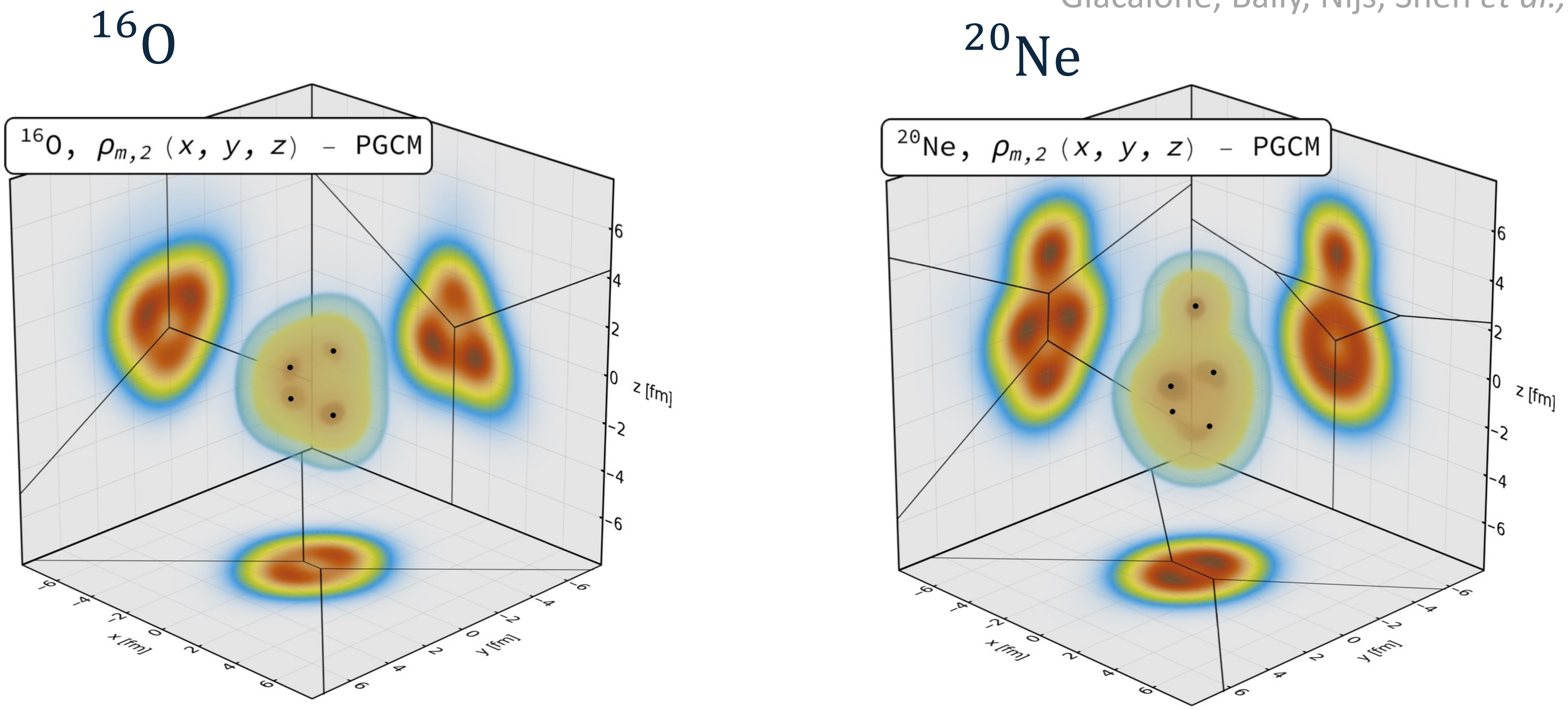

- Ne looks like O, but with an extra α-cluster on top
- Central NeNe/OO v_2 ratio should have a large signal

Central NeNe/OO v_2 ratio

G. Nijs

SOPHIA HADRON PHYSICS GROUP

Giacalone, Bally, Nijs, Shen *et al.*, 2402.05995

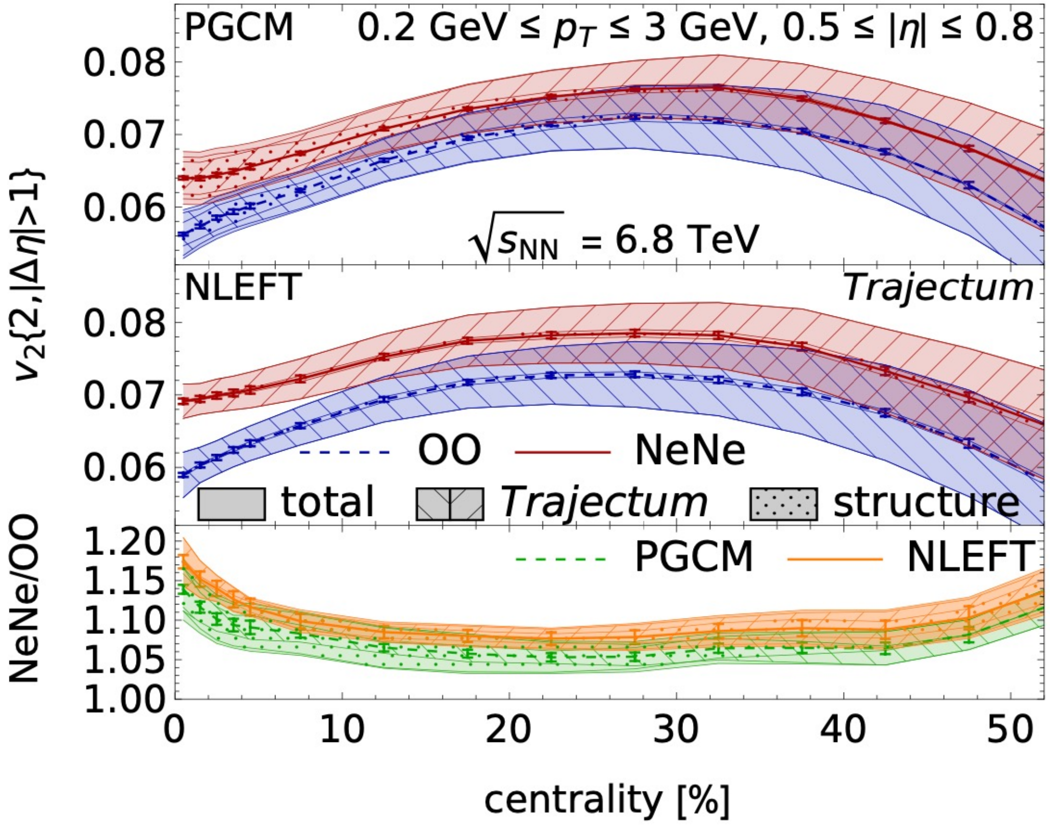

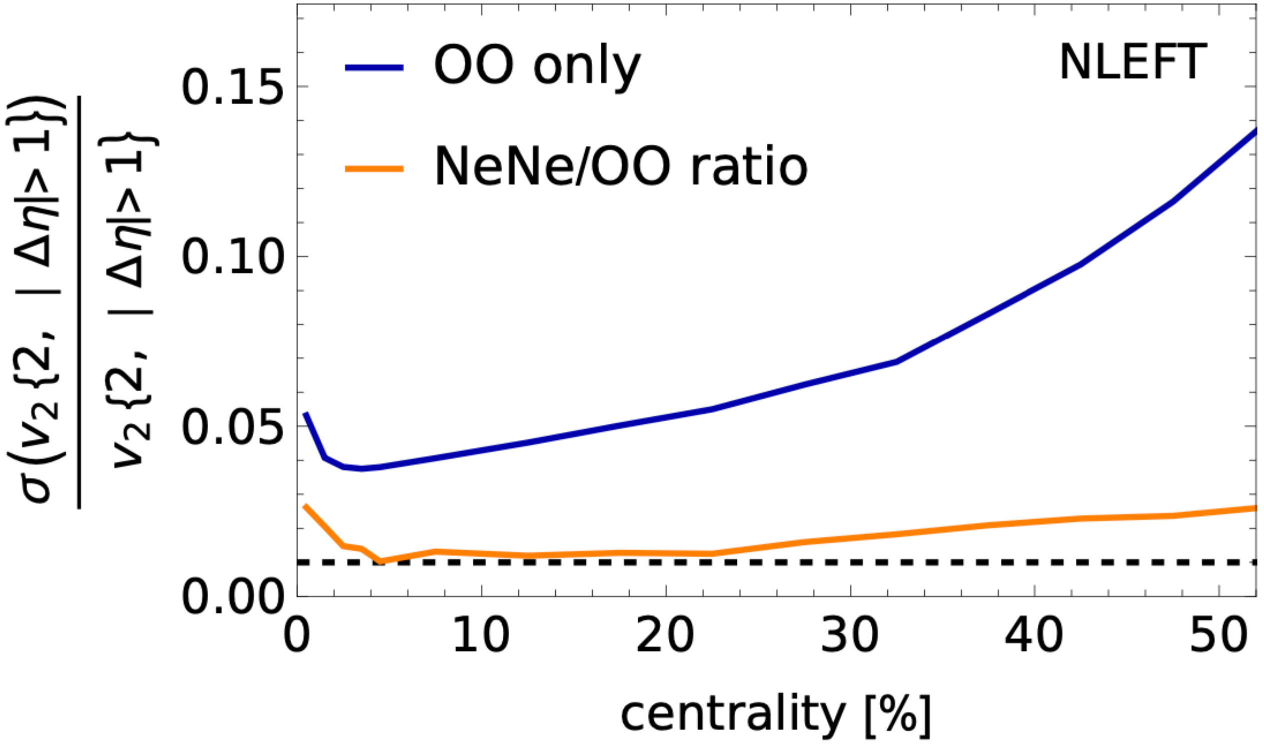

- Central NeNe/OO v_2 ratio has a large enhancement
- Geometric uncertainties indeed largely cancel

Opportunity at LHCb SMOG experiment

C. Shen

SOPHIA HADRON PHYSICS GROUP

Pb + X collisions (fixed-target)

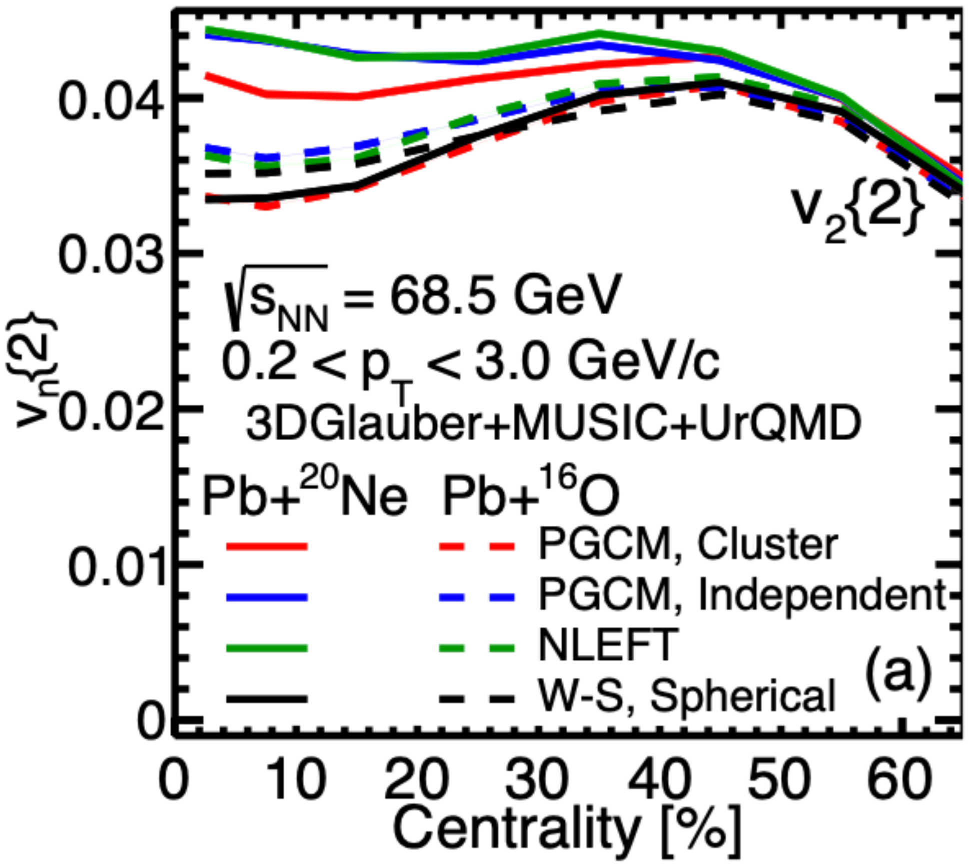

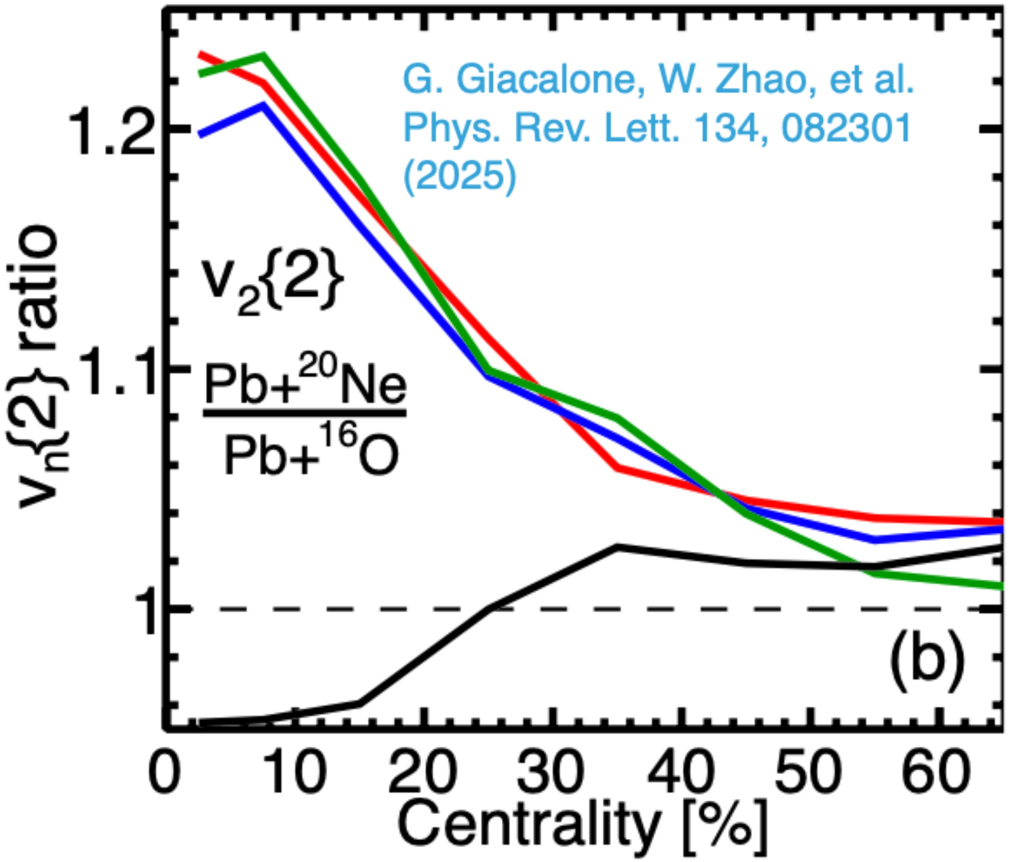

Pb+Ne

Pb+O

- Strong impact of the shape of Ne (~20% enhancement)
- The signal survives up to large centralities

Rapidity scan with DCCI at LHC energy

Based on:

Shin-ei Fujii (poster 2, Tue)

Rapidity Scan

S. Fujii

SOPHIA HADRON PHYSICS GROUP

Expected high baryon number density in forward rapidity in high-energy collisions

M. Li and J. I. Kapusta, Phys. Rev. C **99**, 014906 (2019)

Rapidity Scan

Access high baryon chemical potential region in the QCD phase diagram

Beam Energy Scan @ low energy ⟷ **Rapidity Scan @ high energy**

Complementary study of QCD phase diagram by BES and Rapidity Scan!

QCD phase diagram and experiments

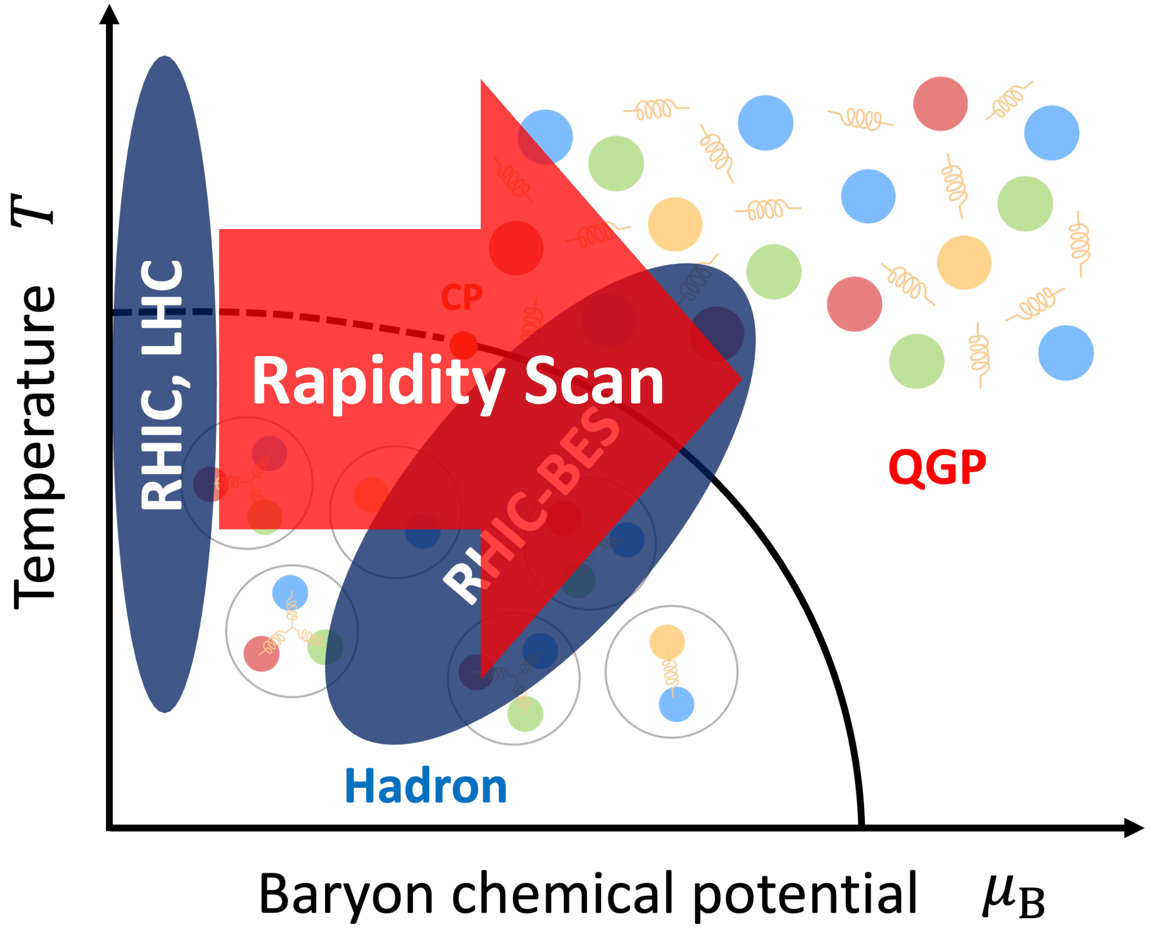

A fundamental question

S. Fujii

SOPHIA HADRON PHYSICS GROUP

How large baryon chemical potential is achieved as equilibrated matter in forward rapidity?

To answer the question, models must describe…

- Equilibrium and non-equilibrium components separately
- Fluidization (equilibration) of baryon number
- Hydrodynamic evolution of baryon number density

→ **DCCI + finite n_{B} extension**

Dynamical Core-Corona Initialization model

S. Fujii

Y. Kanakubo *et al.*, Phys. Rev. C **105**, 024905 (2022)

Initial partons

by PYTHIA8/PYTHIA8 Angantyr

T. Sjöstrand *et al.*, Comput. Phys. Commun. 191, 159 (2015)
C. Bierlich *et al.*, JHEP 1610, 139 (2016)

Dynamical initialization

through the energy-momentum source term j^ν

Core-corona picture

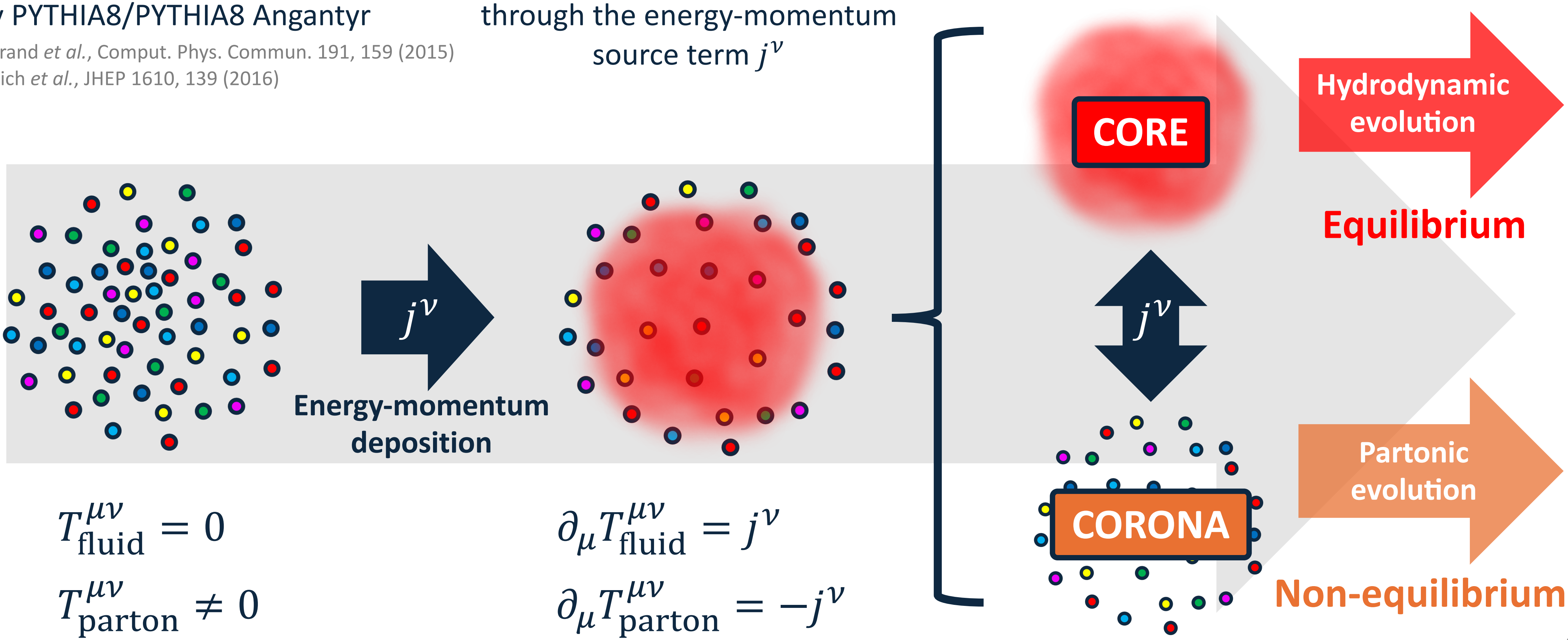

$$T^{\mu\nu}_{\text{fluid}} = 0$$
$$T^{\mu\nu}_{\text{parton}} \neq 0$$

$$\partial_\mu T^{\mu\nu}_{\text{fluid}} = j^\nu$$
$$\partial_\mu T^{\mu\nu}_{\text{parton}} = -j^\nu$$

Source terms

S. Fujii

SOPHIA HADRON PHYSICS GROUP

Energy-momentum source term

Y. Kanakubo *et al.*, Phys. Rev. C **105**, 024905 (2022)

$$\partial_\mu T^{\mu\nu}_{\mathrm{fluid}} = j^\nu$$

$$j^\nu = -\sum_i^{N_{\mathrm{parton}}} \boxed{\frac{dp_i^\nu(t)}{dt}} G(\boldsymbol{x} - \boldsymbol{x}_i(t))$$

p_i^ν: Four-momentum of ith parton

G: Gaussian function $\boldsymbol{x}_i$: Position of ith parton

When ith parton deposits all energy = dead parton

New!!

Conserved charge source term

$$\partial_\mu N^{\mu}_{\mathrm{fluid,\,I}} = \rho_{\mathrm{I}} \qquad \mathrm{I: B, Q, S}$$

$$\rho_{\mathrm{I}} = -\sum_j^{N_{\mathrm{dead}}} \frac{dN_{j,\mathrm{I}}}{dt} G\left(\boldsymbol{x} - \boldsymbol{x}_j(t)\right)$$

$N_{j,\mathrm{I}}$: Charge I of jth dead parton

- **Phenomenological fluidization rate per particle in core-corona picture**

  Low p_{T} / Dense → **CORE**

  High p_{T} / Dilute → **CORONA**

- **Deposition of conserved charges into the fluid**

  Equilibrated baryon number in CORE

Profiles of CORE

S. Fujii

SOPHIA HADRON PHYSICS GROUP

Pb+Pb 2.76 TeV, b = 2.46 fm, Single event

Temperature (longitudinal)

Temperature (transverse)

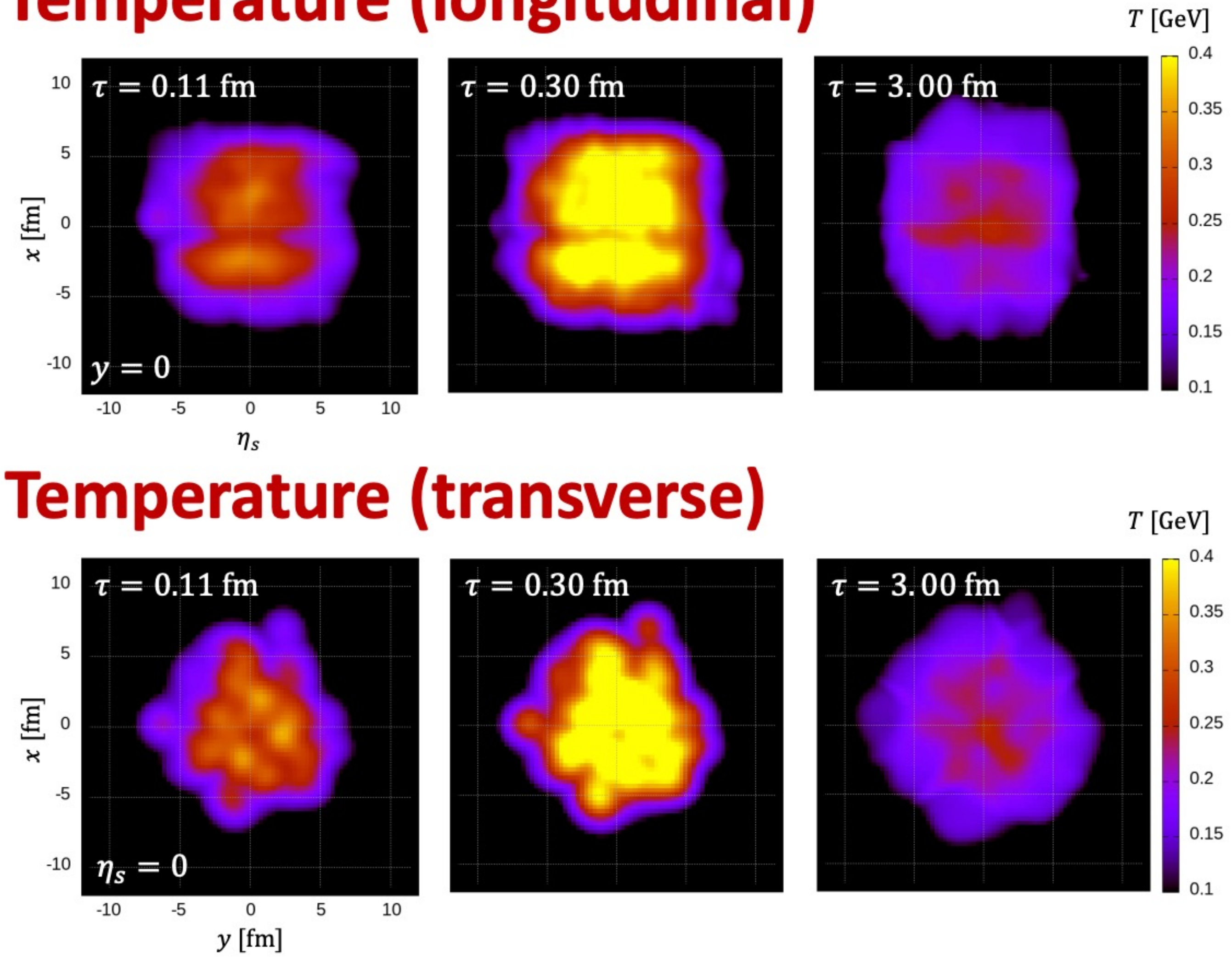

- Gradual formation of the core through the energy-momentum source term
- Alongside the fluid formation, the core expands and cools down due to the hydrodynamic evolution

Fluid formation	+	Fluid evolution
Dominant in early times		Dominant in later times

Profiles of CORE

S. Fujii

SOPHIA HADRON PHYSICS GROUP

Pb+Pb 2.76 TeV, b = 2.46 fm, Single event

Baryon number density (longitudinal)

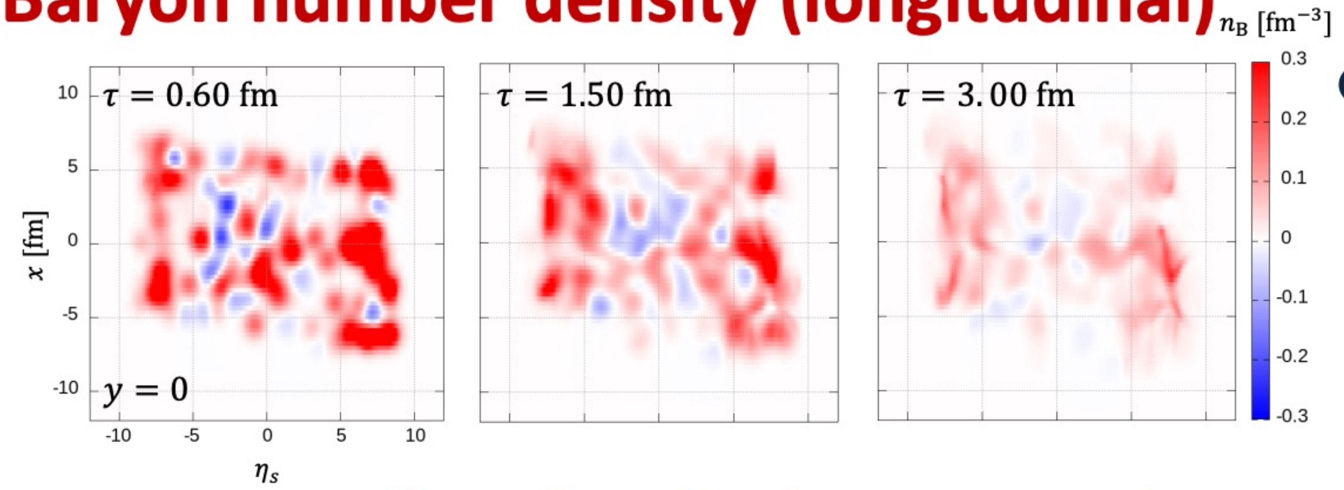

- Large <u>equilibrated</u> baryon number density in forward rapidities
  $$5 \lesssim |\eta_s| \lesssim 10$$
  cf.) $y_{\rm beam}(\sqrt{s_{\rm NN}} = 2.76\ {\rm TeV}) \approx 8$

Baryon number density (transverse)

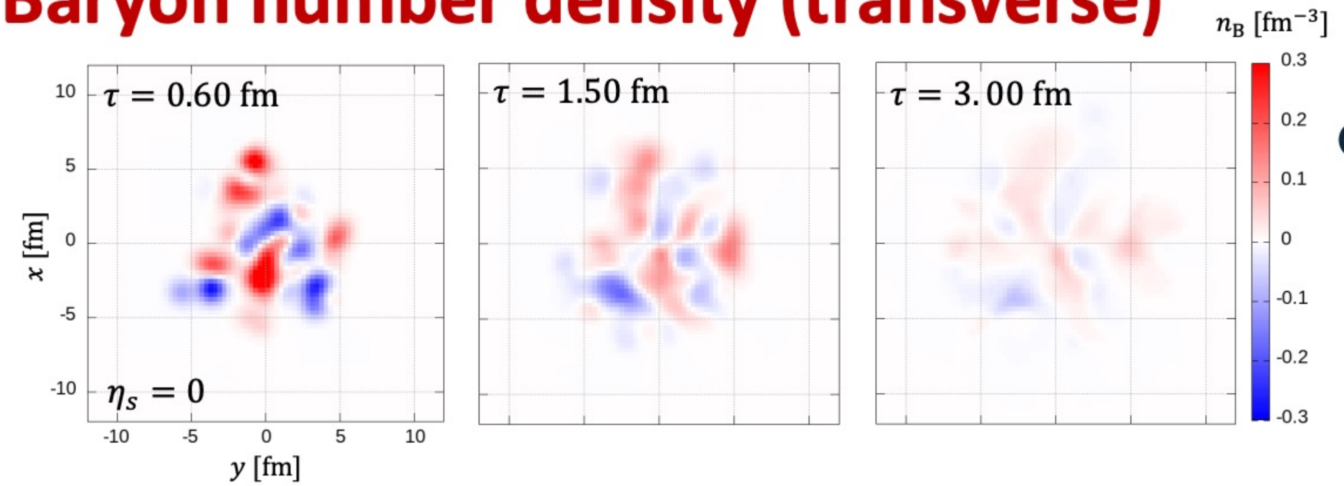

- Large <u>fluctuations</u> of baryon number density in midrapidity

  ➡ Negative n_B regions appear

Freezeout hypersurface

S. Fujii

SOPHIA HADRON PHYSICS GROUP

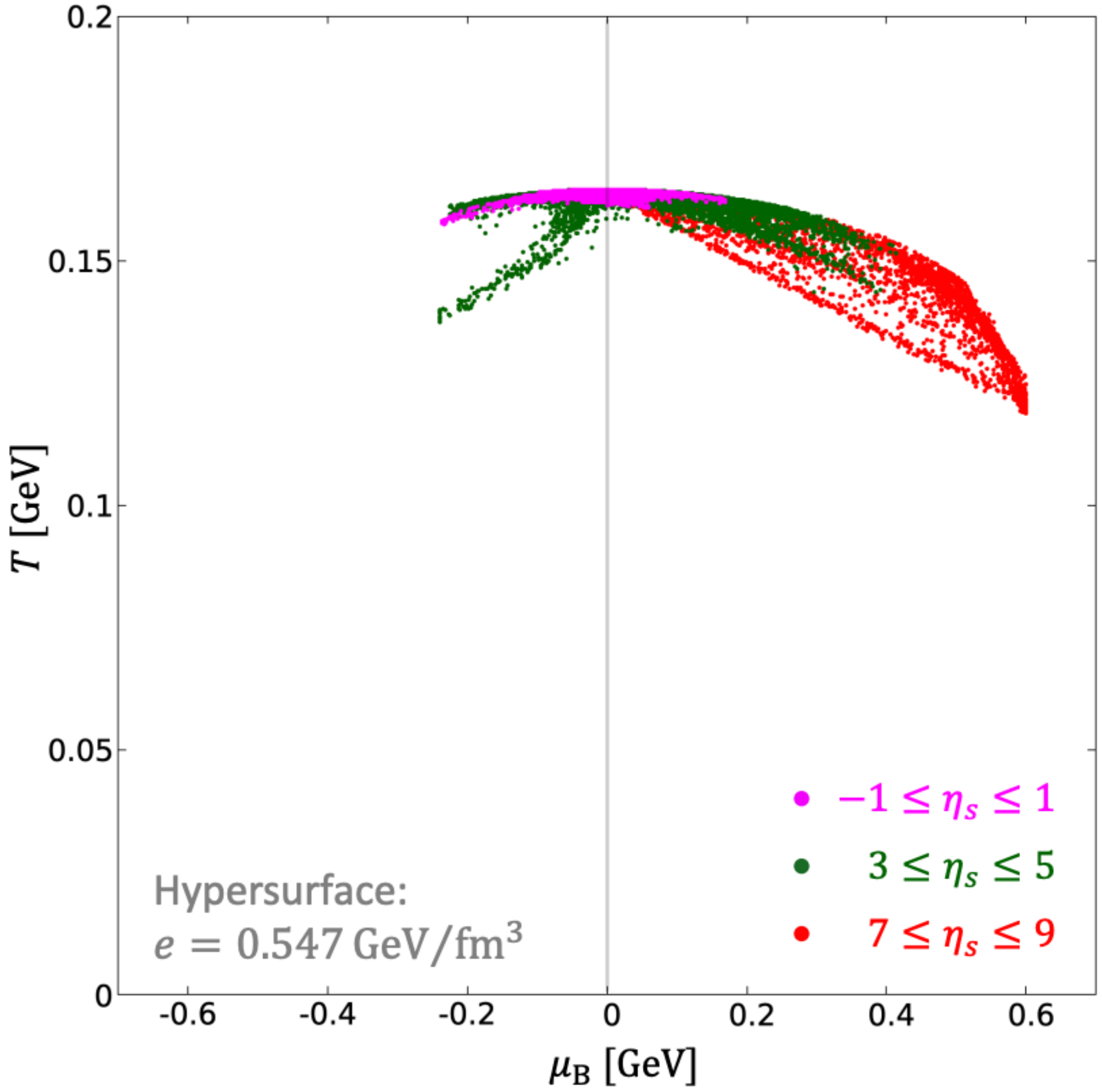

- Large fluctuations of baryon chemical potentials even in midrapidity

$$-0.2 \lesssim \mu_B \lesssim 0.2\ \mathrm{GeV}$$

- Typical baryon chemical potentials increase as go forward rapidity

- Significantly large baryon chemical potentials in forward rapidities

$$\mu_B \lesssim 0.6\ \mathrm{GeV}$$

Averaged freezeout hypersurface

S. Fujii

SOPHIA HADRON PHYSICS GROUP

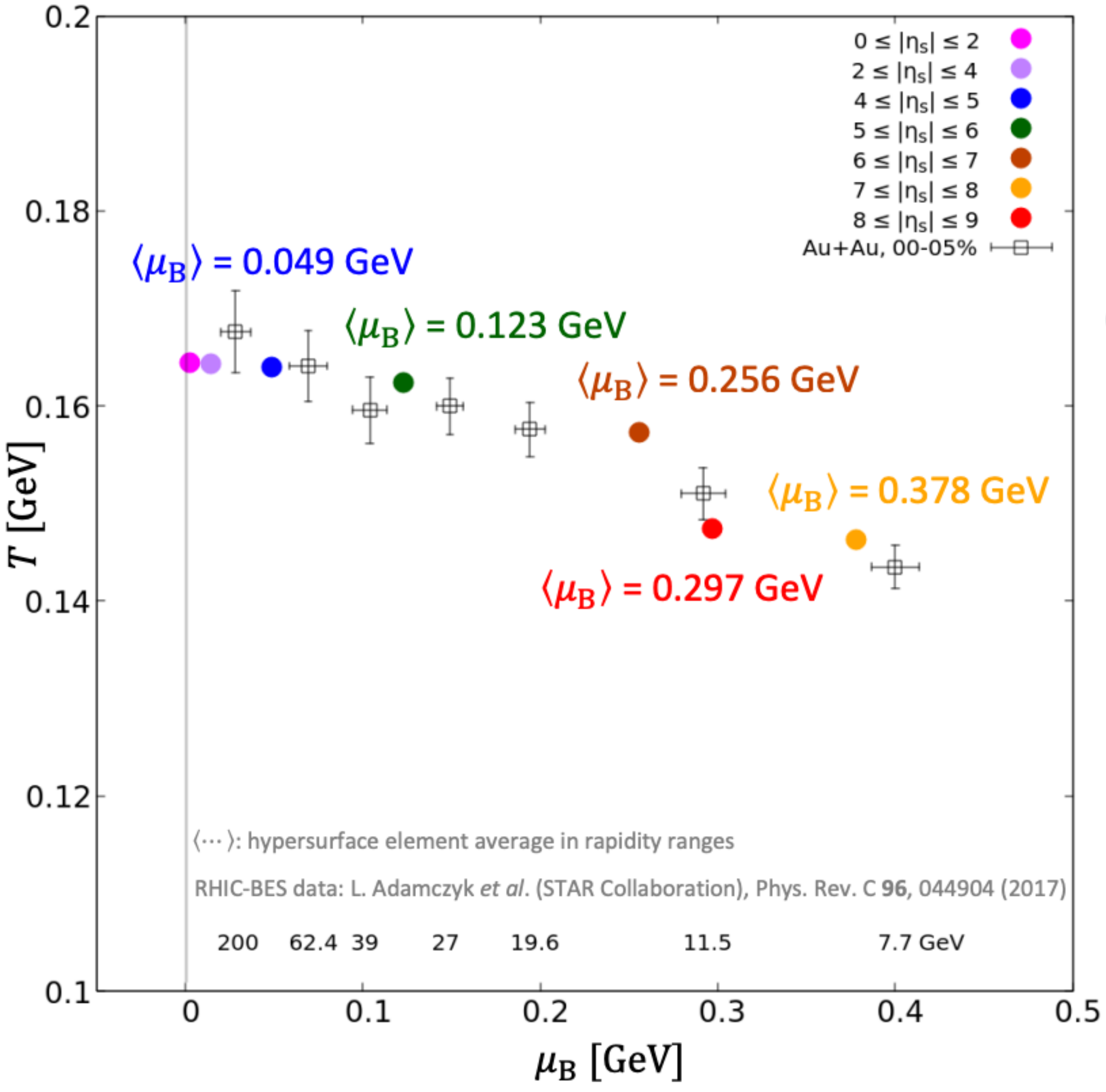

- Baryon chemical potentials increase as one goes forward rapidity
  - ➡ peak at $7 \le |\eta_s| \le 8$
- Almost zero baryon chemical potentials until $|\eta_s| \le 4$
  - ➡ ≈ Au+Au 200 GeV
- Averaged-hypersurface in rapidity range $7 \le |\eta_s| \le 8$ exceeds $\mu_B = 300$ MeV
  - ➡ ≈ Au+Au 7.7 GeV

Rapidity Scan is a new possible tool for exploring the QCD phase diagram

Backups

Other interesting topics of hydrodynamics

SOPHIA HADRON PHYSICS GROUP

- Stochastic hydrodynamics (N. Mullins, D. Teaney)
- Spin hydrodynamics (D. Wagner)
- Hydrodynamics of heavy quarks (F. Capellino)
- Magneto hydrodynamics (A. Dash)
- Hydrodynamic description of initial stage (A. Kirchner)

Numerical stabilization

L. Gavassino

In the equation of motion for the stress ($\boldsymbol{\tau_\Pi \dot{\Pi} + \Pi = -\zeta \partial_\mu u^\mu}$), the velocity gradient is treated as a source, but it contains time derivatives.

This requires a two-step initialization ($\boldsymbol{\Psi_\mathrm{n}}$ ≡"variables at time-step $\boldsymbol{n\Delta t}$"):

$\boldsymbol{\Psi_{-1}}$ ="Something"

$\boldsymbol{\Psi_0}$ ="Initial data"

Current codes set $\boldsymbol{\Psi_{-1} = \Psi_0}$, which is inconsistent with the equations of motion $\boldsymbol{\partial_t \Psi = F(\Psi, \partial_j \Psi)}$. We should set

$$\boldsymbol{\Psi_{-1} \approx \Psi_0 - \Delta t\, F(\Psi_0, \partial_j \Psi_0)}$$

When we do it, the code crashes as it should! **(Details are code-dependent)**

Nuclear structure from isobar collisions

C. Shen

SOPHIA HADRON PHYSICS GROUP

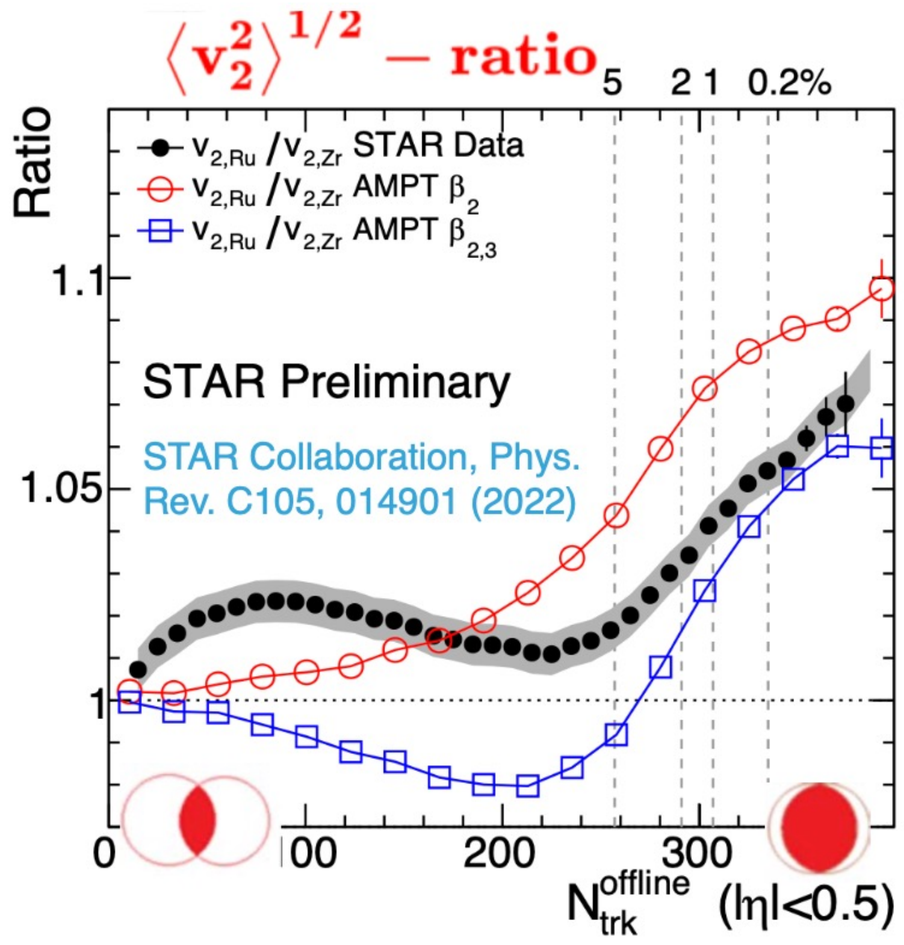

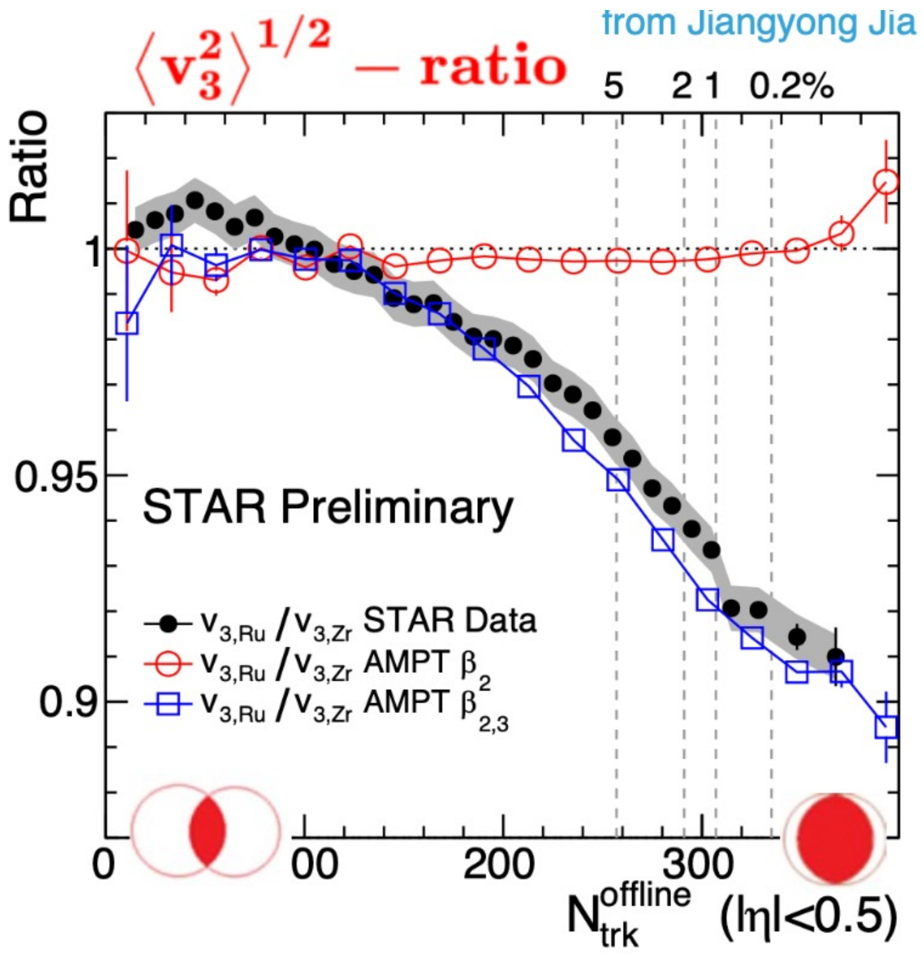

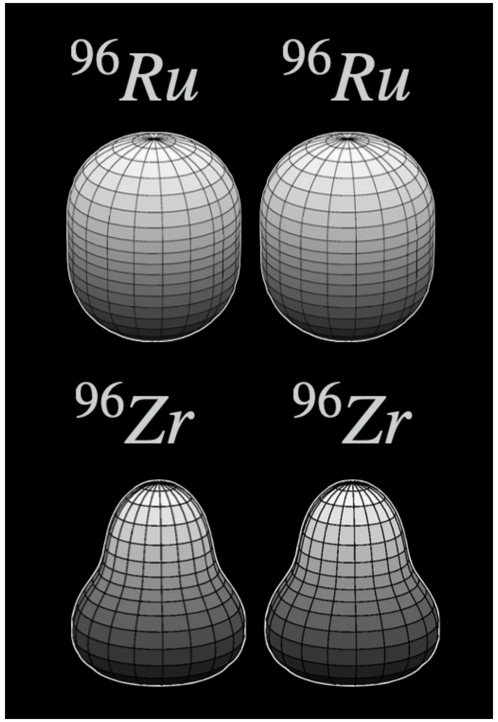

Dependence on nuclear structure of ^{16}O

X. Zhao

SOPHIA HADRON PHYSICS GROUP

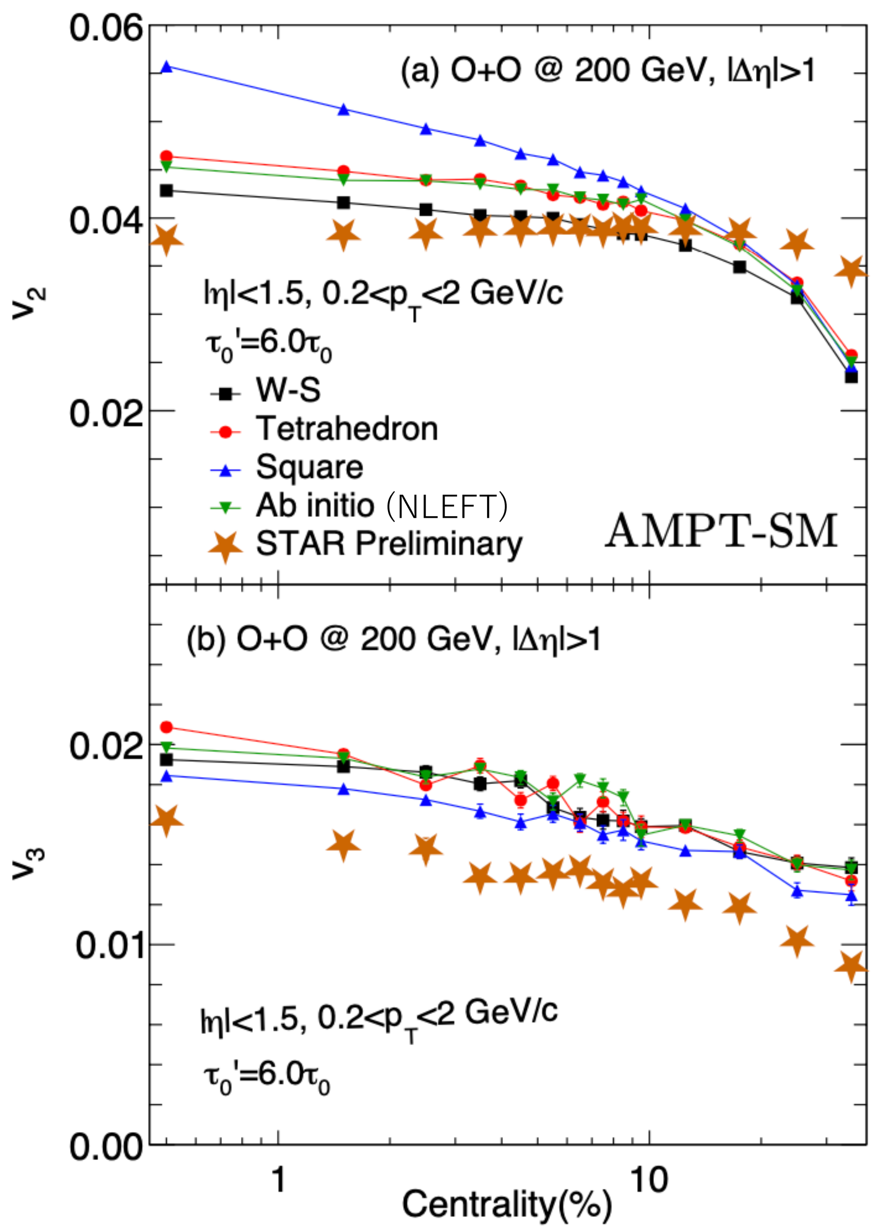

Xin-Li Zhao(poster1, Tue)

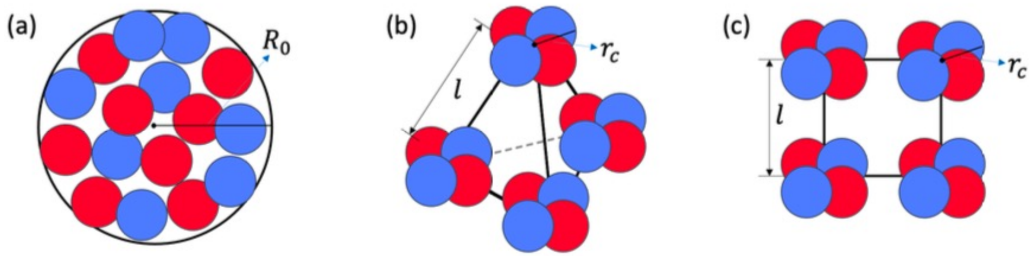

- The square configuration shows the largest v_2
- The W-S configuration shows the smallest v_2
- Overestimate the STAR data

Changing signatures of α-clustering

C. Shen

SOPHIA HADRON PHYSICS GROUP

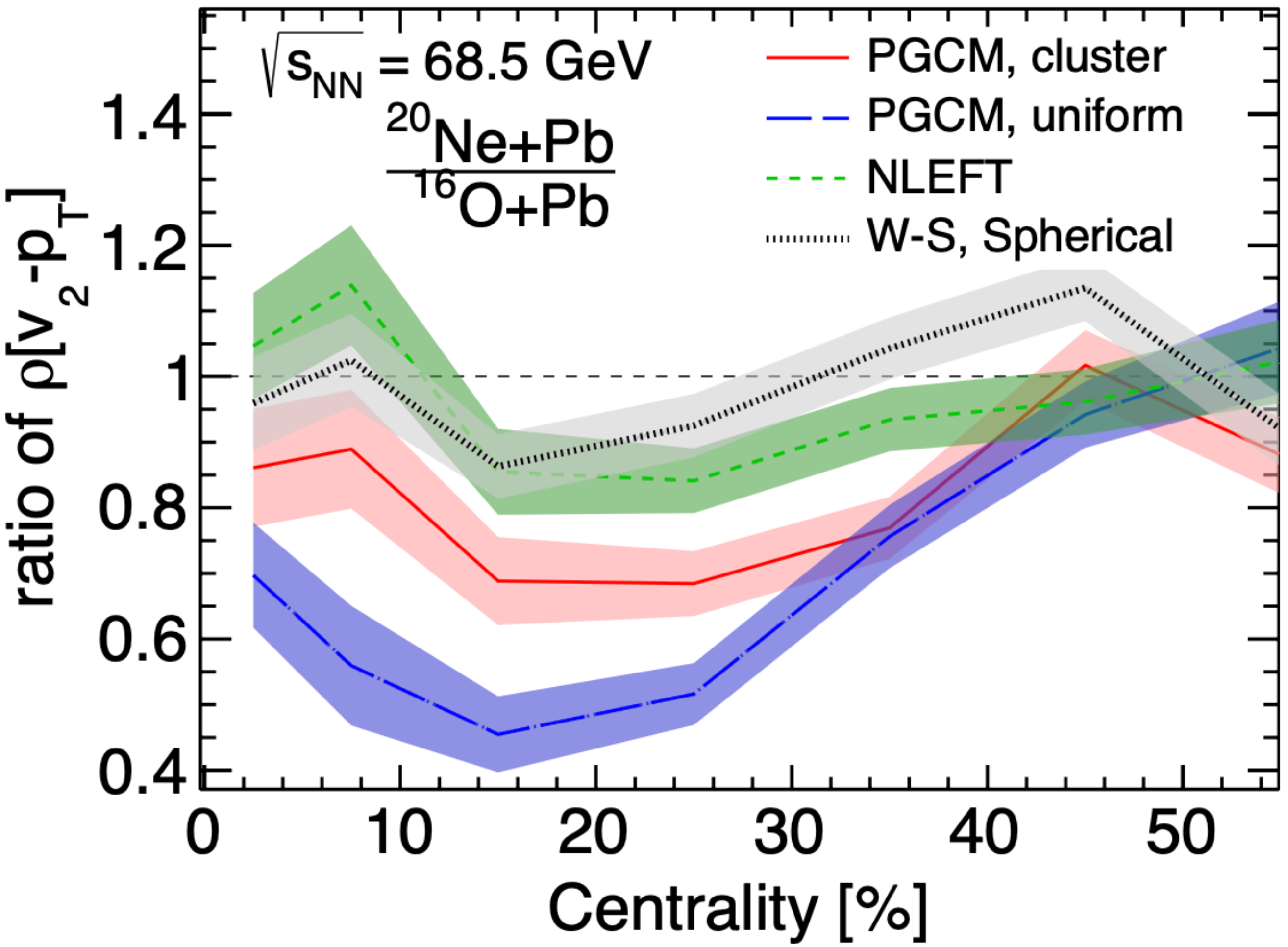

$$\rho(v_n^2, \langle p_T \rangle) = \frac{\left\langle \hat{\delta} v_n^2 \hat{\delta} \langle p_T \rangle \right\rangle}{\sqrt{\left\langle \left(\hat{\delta} v_n^2\right)^2 \right\rangle \left\langle \left(\hat{\delta} \langle p_T \rangle\right)^2 \right\rangle}}$$

The ratios of v_2 - p_T correlation show sensitivity to nuclear configurations from different low-energy nuclear theory calculations

NLEFT and PGCM

Giacalone, Bally, Nijs, Shen *et al.*, 2402.05995

Nuclear Lattice Effective Field Theory

$^{16}\mathrm{O}$

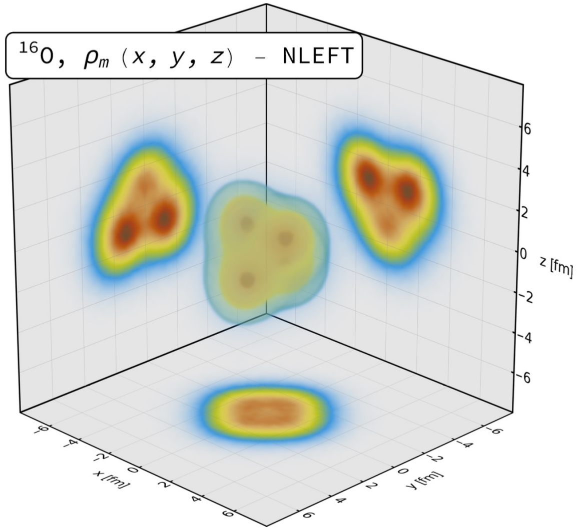

$^{20}\mathrm{Ne}$

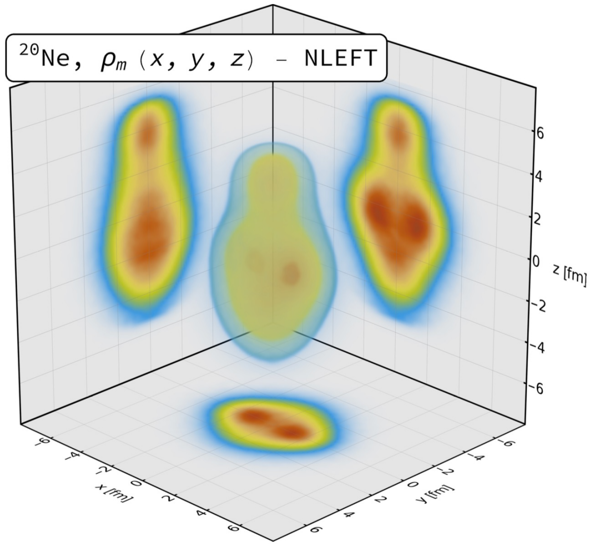

ab initio
Projected Generator Coordinate Method

$^{16}\mathrm{O}$

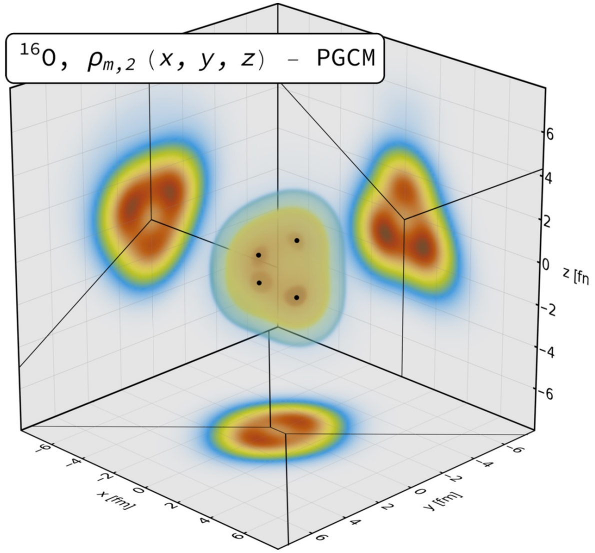

$^{20}\mathrm{Ne}$

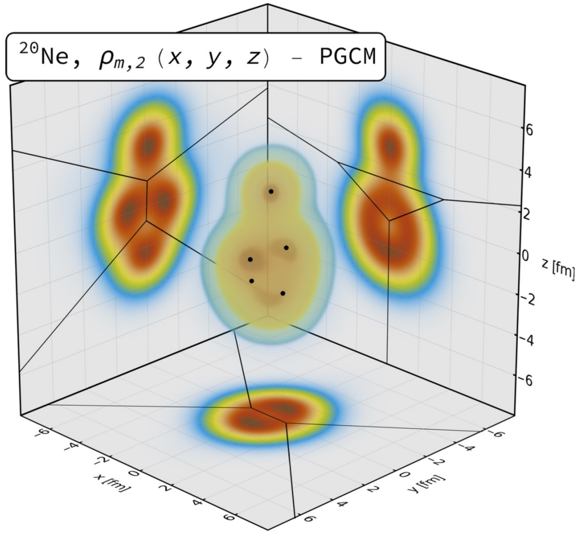

- Nuclei from both models look quite similar